the plant journal

SEB SOCIETY FOR EXPERIMENTAL BIOLOGY

The Plant Journal (2025) **121,** e17194 doi: 10.1111/tpj.17194

miR158a negatively regulates plant resistance to *Phytophthora parasitica* by repressing AtTN7 that requires EDS1-PAD4-ADR1 complex in *Arabidopsis thaliana*

Yilin Li[1], Xiuhong Gou[2], Ruize Ma[1], Peiling Zhang[1], Assiya Ansabayeva[3], Qingyao Shi[1], Zeming Liu[1], Yuling Meng[1] and Weixing Shan[1,*]

[1]*State Key Laboratory of Crop Stress Resistance and High-Efficiency Production, and College of Agronomy, Northwest A&F University, Yangling, Shaanxi 712100, China,*

[2]*State Key Laboratory of Crop Stress Resistance and High-Efficiency Production, and College of Plant Protection, Northwest A&F University, Yangling, Shaanxi 712100, China, and*

[3]*Department of Agronomy, A. Baitursynov Kostanay Regional University, Kostanay 110000, Republic of Kazakhstan*

Received 26 August 2024; revised 18 November 2024; accepted 25 November 2024; published online 5 December 2024.
*For correspondence (e-mail wxshan@nwafu.edu.cn).

SUMMARY

Small RNAs are involved in diverse cellular processes, including plant immunity to pathogens. Here, we report that miR158a negatively regulates plant immunity to the oomycete pathogen *Phytophthora parasitica* in *Arabidopsis thaliana*. By performing real-time quantitative PCR, transient expression, and RNA ligase-mediated 5′ rapid amplification of cDNA ends assays, we demonstrate that miR158a downregulates *AtTN7* expression by cleaving its 3′-untranslated region. *AtTN7* positively affects plant immunity and encodes a truncated intracellular nucleotide-binding site and leucine-rich repeat receptor containing the Toll/interleukin-1 receptor. AtTN7 can degrade oxidized forms of nicotinamide adenine dinucleotide (NAD+). Further genetic and molecular analyses reveal that the Enhanced Disease Susceptibility 1-Phytoalexin Deficient 4-Activated Disease Resistance 1 complex is required for AtTN7-mediated immunity. ADR1-dependent Ca^{2+} influx is crucial for activating salicylic acid signaling to condition AtTN7-triggered immunity. Our study uncovers the immune roles and regulatory mechanisms of miR158a and its target *AtTN7*. Both miR158a-downregulation and *AtTN7*-overexpression lead to enhanced plant resistance to *P. parasitica* without affecting plant growth phenotypes, suggesting their application potentials and the utilization of miRNAs in identifying novel immune genes for the development of plant germplasm resources with enhanced disease resistance.

Keywords: *Arabidopsis thaliana*, *Phytophthora parasitica*, miR158a, *AtTN7*, plant immunity, NAD+ degrade, EDS1-PAD4-ADR1 complex, Ca^{2+} influx, SA signaling.

INTRODUCTION

Oomycetes are an important group of filamentous eukaryotic microorganisms that are morphologically similar to filamentous fungi but phylogenetically more closely related to diatoms and brown algae (Kamoun et al., 2015; Thines, 2018). *Phytophthora* translates to "plant destroyer" and can cause severe losses in agricultural production and destruction in natural ecosystems. A notable example is the Irish Potato Famine in the 1840s that was caused by the potato late blight pathogen *P. infestans*. This pathogen remains a major constraint to potato production, the world's third-largest staple crop (Avila-Quezada & Rai, 2023). Nearly all 180 species in the genus *Phytophthora* are plant pathogens (Kronmiller et al., 2023). They are notorious in that they frequently overcome host genotype-specific genetic resistance, thus necessitating reliance on fungicides to control their respective crop diseases (Sharma et al., 2021). Creative genetic solutions, derived from understanding of plant susceptibility, are therefore promising strategies to provide crop protection. Several negative regulators of plant immunity to *Phytophthora* have been identified, with their conserved immune functions revealed (Li et al., 2020, 2022; Lu et al., 2020; Pan et al., 2016; Yang et al., 2022), implicating their potential in improving disease resistance in multiple crops.

MicroRNAs (miRNAs) in eukaryotes can induce transcriptional or post-transcriptional gene silencing (TGS or PTGS), including in the regulation of plant immune

response to pathogens (Islam et al., 2018; Song et al., 2021). Studies have shown that some plants endogenous miRNAs can be induced by infection of oomycetes and are involved in the regulation of plant immune responses (Cui, Yan, et al., 2017; Gou et al., 2022; Luan et al., 2018). miR158 is found in different plant species, such as *Arabidopsis lyrate* (Fahlgren et al., 2007), *Brassica napus* (Xu et al., 2012), *Brassica oleracea* (Wang et al., 2012), *Raphanus sativus* (Wang et al., 2015), and *Ipomoea batatas* (Sun et al., 2022). miR158 is reported to function in pollen development by targeting pentatricopeptide repeat (PPR) containing protein transcripts in *Brassica campestris* (Ma et al., 2017), to regulate miR173-initiated trans-acting cascade silencing in Indian Himalayan natural *Arabidopsis thaliana* accessions (Tripathi et al., 2023), and to respond to abiotic stress in *I. batatas* (Sun et al., 2022). However, whether miR158a plays regulatory role in plant resistance against pathogens remains largely elusive.

Nucleotide-binding leucine-rich repeat (NLR) proteins are intracellular immune receptors that play critical roles in innate immunity in plants and animals (Maruta et al., 2022). In plants, the typical NLRs have a central nucleotide-binding site (NBS) domain, a C-terminal leucine-rich repeat (LRR) domain, and a N-terminal coiled-coil (CC) or Toll/interleukin-1 receptor (TIR) domain, known as CNL or TNL, respectively (Wang et al., 2020). In addition to the canonical TNLs, *A. thaliana* ecotype Col-0 has been identified to contain 21 truncated TIR-NBS (TN) proteins without the C-terminal LRR domain (Lapin et al., 2022; Li et al., 2015; Meyers et al., 2002; Nandety et al., 2013). Studies have shown that TN proteins play important roles in plant immunity (Nasim et al., 2020; Roth et al., 2017; Wang et al., 2019; Zhao et al., 2015).

Plant TIR proteins can cleave nicotinamide adenine dinucleotide in its oxidized form (NAD+) to produce pRib-ADP, pRib-AMP, ADPR-ATP, di-ADPR, and a variant of cyclic ADP-ribose (v-cADPR) (Duxbury et al., 2020; Huang et al., 2022; Jia et al., 2022; Ma et al., 2020; Song et al., 2024; Wan et al., 2019). Plant TIR-dependent immune signaling relies on downstream conserved helper NLRs (hNLRs). hNLRs can be divided into two groups, one is the lipase-like protein family including Enhanced Disease Susceptibility 1 (EDS1), Phytoalexin Deficient 4 (PAD4) and Senescence-Associated Gene 101 (SAG101), and the other is the CNL class containing N Requirement Gene 1 (NRG1) and Activated Disease Resistance 1 (ADR1) (Dongus & Parker, 2021; Feehan et al., 2020; Huang et al., 2022; Lapin et al., 2022). In *A. thaliana*, a functional partnership of EDS1-PAD4 with ADR1 and EDS1-SAG101 with NRG1 has been reported (Castel et al., 2019; Huang et al., 2022; Jia et al., 2022; Saile et al., 2020; Sun et al., 2021). The assembled EDS1 complex combines with different NAD+ cleavage products to mediate immune responses (Essuman et al., 2022; Huang et al., 2022; Jacob et al., 2021; Jia et al., 2022).

AtTN7 is clustered with eight other TN genes (*AtTN4*–*AtTN12*) on chromosome 1, which is the largest TN cluster (Chen et al., 2021). *AtTN2* also locates on chromosome 1, and phylogenetic analysis shows that AtTN6, AtTN7, AtTN11, and AtTN12 are highly homologous to the AtTN2 protein (Meyers et al., 2002). Among these "AtTN2" proteins, AtTN2, AtTN11, and AtTN12 are confirmed to trigger cell death, while the AtTN6 could not be amplified from *A. thaliana* leaves (Chen et al., 2021). Moreover, AtTN2 is reported to mediate spontaneous cell death and enhance plant resistance to powdery mildew pathogen *Golovinomyces cichoracearum*, and ADR1s are required for the TN2-meditaed immune responses (Wang et al., 2021). *AtTN11* functional deficiency results in reduced plant resistance against *Pseudomonas syringae* pv. *tomato* (Pto) (Nasim et al., 2020). Interestingly, compared with AtTN2, AtTN11, and AtTN12, AtTN7 is unable to induce cell death (Chen et al., 2021). However, how *AtTN7* is involved in regulating plant immunity has not yet been elucidated. AtTN7 carries conserved TIR and NBS domains, which are required for cleaving NAD+, sensing pathogen infection, and transmitting plant immune signals (Liu et al., 2023; Song et al., 2024; Wan et al., 2019). Nevertheless, whether AtTN7 has the ability to degrade NAD+ remains unclear. In addition, whether and which hNLRs participate in AtTN7-mediated plant resistance remains unknown.

In this study, we show that miR158a negatively regulates plant immunity to *Phytophthora parasitica* by cleaving *AtTN7* transcripts. We further demonstrate that AtTN7 can degrade NAD+ and AtTN7-mediated plant resistance to *P. parasitica* is closely associated with its NADase activity and EDS1-PAD4-ADR1 complex. Our study reveals the immune roles and regulatory mechanisms of miR158a and *AtTN7*. miR158a-mediated cleavage of *AtTN7* transcripts resulted in the suppression of helper NLR EDS1-PAD4-ADR1 complex and associated SA signaling, leading to enhanced plant susceptibility.

RESULTS

miR158a negatively regulates plant immunity to *P. parasitica*

Previous sequencing data showed that *A. thaliana* miR158a was differentially expressed at different time points of *P. parasitica* infection as compared to mock-inoculated plants (Zhong, 2019). Stem-loop real-time quantitative PCR (RT-qPCR) analyses showed that the expression of miR158a in leaf tissue was slightly induced at 3 and 6 h post-inoculation (hpi), highly induced at 12 hpi (Figure S1). We thus speculated that miR158a may be involved in *A. thaliana* defense response against *P. parasitica*.

To examine the role of miR158a in plant immune response to *P. parasitica*, we obtained three different miR158a silence lines (*mir158a-ti2*, *mir158a-ko12*, and

mir158a-st12). *mir158a-ti2* is a T-DNA insertion mutant (SALK_031515C) with an insertion site downstream of mature miR158a (Figure 1a), *mir158a-ko12* is a knockout mutant generated by CRISPR/Cas9-based genome editing (Figure 1b), and *mir158a-st12* is a silenced transgenic line obtained via G:U hpRNA sponge tool used in previous study (Gou et al., 2022). Stem-loop RT-qPCR results showed that the expression level of miR158a was significantly decreased in three different miR158a silence lines (Figure 1c). Inoculation assays with *P. parasitica* revealed that *mir158a-ti2*, *mir158a-ko12*, and *mir158a-st12* plants were more resistant to *P. parasitica* than wild-type Col-0 plants, and these lines exhibited limited *P. parasitica* colonization (Figure 1d–f). We also generated transgenic plants that overexpressed miR158a in Col-0 background. The expression level of miR158a was greatly increased in MIR158a-OE3 and MIR158a-OE18 (Figure 1c), and these two miR158a-overexpressing lines showed enhanced susceptibility to *P. parasitica*, and *P. parasitica* colonization was greater compared to Col-0 (Figure 1d–f). These results

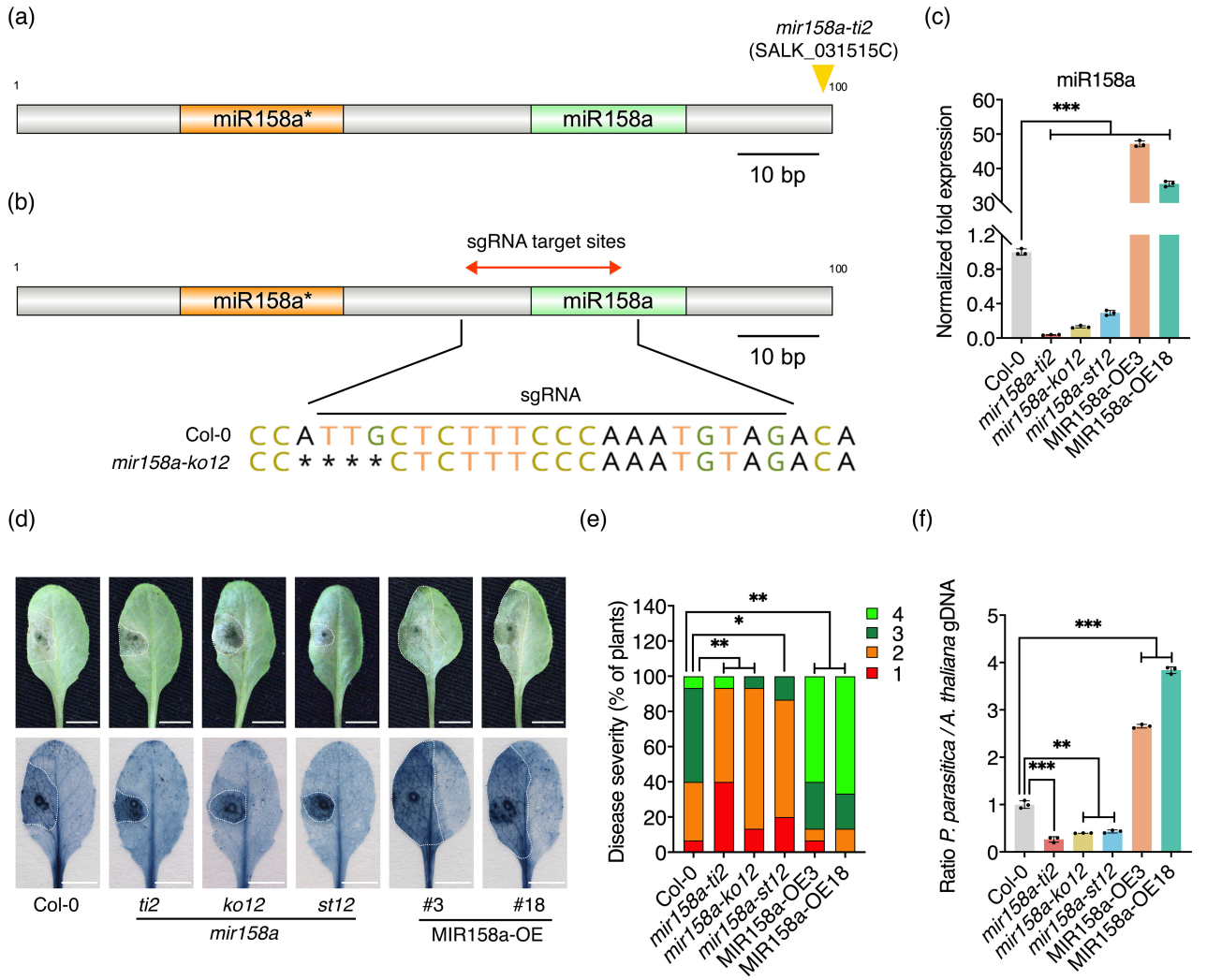

Figure 1. miR158a mediates *Arabidopsis thaliana* susceptibility to *Phytophthora parasitica*.
(a) Schematic diagram of the T-DNA insertion site of *mir158a-ti2*. The T-DNA of *mir158a-ti2* is inserted into downstream of mature miR158a.
(b) Schematic representation of the editing sites in the miR158a CRISPR/Cas9 mutant. The *mir158a-ko12* mutant has a deletion of four bases. The red arrow indicates editing sites, and the black asterisks indicate deletion positions.
(c) Relative expression level of miR158a in *mir158a* mutants and MIR158a-OE lines. The expression level was determined by stem-loop RT-qPCR, with *A. thaliana U6* (*AtU6*) as an internal reference. Results are shown as the mean ± SD ($n = 3$).
(d) Disease lesions of *mir158a* mutants and MIR158a-OE lines infected with *P. parasitica* zoospores at 3 days post-inoculation (dpi). The water-soaked lesions were colored by trypan blue staining. Scale bars: 5 mm.
(e) Disease severity in infected leaves was evaluated by calculating the proportion of lesion area to leaf area at 3 dpi. Grade 1, 0–10%; 2, 10–33%; 3, 33–66%; and 4, 66–100%. Wilcoxon rank-sum test was used for data analysis. At least three independent experiments were performed.
(f) The *P. parasitica* biomass in infected leaves was quantified by quantitative PCR (qPCR) at 3 dpi. Results are shown as the mean ± SD ($n = 3$). The statistical analysis of (c) and (f) was conducted with Student's *t*-test. Asterisks indicate significant differences (*$P < 0.05$, **$P < 0.01$, ***$P < 0.001$).

demonstrated that miR158a inhibited plant resistance to *P. parasitica*.

miR158a represses *AtTN7* expression

We predicted that miR158a potentially targeted the 3′-untranslated region (3′-UTR) of *AtTN7*, using psRNATarget (http://plantgrn.noble.org/psRNATarget) (Dai & Zhao, 2011). To verify miR158a-mediated suppression of *AtTN7*, we examined *AtTN7* transcripts in *mir158a* mutants and MIR158a-OE lines. RT-qPCR results showed that *AtTN7* transcripts level was upregulated in *mir158a* mutants and downregulated in MIR158a-OE lines, and the change in *AtTN7* expression was more significant at 12 hpi with *P. parasitica* compared to the un-inoculated (Figure 2a,b). Furthermore, the expression of miR158a was negatively correlated with *AtTN7* during *P. parasitica* infection (Figure 2c).

To further confirm the target site, we performed GFP-based reporter assays. Considering that the predicted target site of miR158a was located in the 3′-UTR of *AtTN7*, we generated constructs to fuse GFP with the 3′-UTR of *AtTN7* (*GFP-AtTN7*-wtUTR). Separately, we also mutated the 3′-UTR of *AtTN7* (*GFP-AtTN7*-muUTR) to abolish complementarity to miR158a (Figure 2d). We co-expressed the constructs with pre-miR158a (*35S::miR158a*) or mature miR158a (amiR158a) (Schwab et al., 2006) in *Nicotiana benthamiana*, fluorescence intensity and Western blot analysis revealed that when *GFP-AtTN7*-wtUTR and *GFP-AtTN7*-muUTR were expressed alone, their proteins were highly accumulated. Nevertheless, when co-expressed with *35S::miR158a* or amiR158a, and the *Agrobacterium* concentrations of *35S::miR158a* or amiR158a gradually increased, the protein levels of GFP-AtTN7-wtUTR were significantly decreased, but no difference in GFP-AtTN7-muUTR protein levels (Figure 2e–h), elucidating that both pre-miR158a and mature miR158a depressed *AtTN7* expression.

Furthermore, to investigate whether miR158a repressed the expression of *AtTN7* by mRNA cleavage, we performed RNA ligase-mediated 5′ rapid amplification of cDNA ends (RLM-5′ RACE) assays using *P. parasitica*-infected *A. thaliana* leaves at 12 hpi. The cleavage site was determined between the 9th and 10th nucleotides of the paired fragment of miR158a and *AtTN7* (Figure 2i; Figure S2). Taken together, these results confirmed that miR158a suppressed *AtTN7* expression by cleaving the 3′-UTR of *AtTN7* mRNA.

AtTN7 positively affects plant immunity to *P. parasitica*

To explore the role of *AtTN7* during plant immune response, we created two individual *AtTN7* knockout mutants, *tn7-1* and *tn7-4*, employing CRISPR/Cas9-based technology (Figure S3). The transcript level of *AtTN7* was significantly decreased in *tn7-1* and *tn7-4* (Figure 3a). The pathogenicity assays with *P. parasitica* zoospores showed that *tn7-1* and *tn7-4* developed significantly larger lesions and greater *P. parasitica* colonization compared to Col-0 (Figure 3b–d). We also obtained *AtTN7* overexpressing transgenic lines in the Col-0 background. RT-qPCR results showed that the transcript level of *AtTN7* was significantly increased in *TN7*-OE9 and *TN7*-OE11 (Figure 3a). Infection assays showed that *TN7*-OE9 and *TN7*-OE11 developed smaller lesions and less *P. parasitica* colonization than Col-0 (Figure 3b–d). We further expressed *AtTN7* under the control of its native promoter in *tn7-4* mutant background to generate *AtTN7* complementation transgenic lines, *TN7*-CP3 and *TN7*-CP5. The expression of *AtTN7* in *TN7*-CP3 and *TN7*-CP5 significantly recovered as compared to *tn7-4*, being similar to Col-0 (Figure S4a). The leaf inoculation assays showed no significant difference in the size of water-soaked lesions or of *P. parasitica* colonization between *TN7*-CP lines and Col-0, and the susceptibility of *tn7-4* was restored in *TN7*-CP lines (Figure S4b–d). The results strongly supported that *AtTN7* positively regulated plant immunity to *P. parasitica*.

AtTN7 is predicted to encode a Toll/interleukin-1 receptor (TIR)-nucleotide-binding site (NBS) protein. Sequence alignment of AtTN7 with the well-characterized TNL protein L6 and RPS4 (Resistance to *Pseudomonas syringae* 4) (Chen et al., 2021) showed that AtTN7 contained a representative TIR domain with four conserved TIR subdomains (TIR1-TIR4) (Figure S5). In addition, Walker A, Walker B, RNBS-A, RNBS-B and RNBS-C motifs were also observed in the NBS domain of AtTN7, but not highly conserved (Figure S5). We also found that AtTN7 was localized in the cytoplasm and plasma membrane (Figure 3e,f) by transiently co-expressing the fusion construct *GFP-TN7* in *N. benthamiana* with cytoplasm and plasma membrane marker, respectively. Western blot analysis confirmed the protein expression and integrity (Figures S6 and S7).

TIR NADase activity requires the proximity and homodimerization of at least two TIR domains (Lapin et al., 2022). Both *in planta* Co-immunoprecipitation and *in vitro* pull-down assays demonstrated the homodimerization of AtTN7 TIR domains (Figure S8). We found that the conserved catalytic residue (E84), AE interface (S27/F28), and DE interface (G151) are present in AtTN7-TIR (Figure S5), which are essential to the plant TIR domains to act as NADase (Horsefield et al., 2019; Ma et al., 2020; Martin et al., 2020; Nimma et al., 2021; Wan et al., 2019). The difference is that the AE interface in TN proteins is SF (serine and phenylalanine), and it is also involved in a stacking interaction with the equivalent residue in the neighboring interacting molecule (Williams et al., 2014). Plant TIR proteins can cleave NAD+ to produce v-cADPR (Wan et al., 2019), and plant BdTIR has been reported to produce 2′cADPR (major) and 3′cADPR (minor) (Bayless et al., 2023; Wan et al., 2019). To characterize reaction products of AtTN7-TIR, we purified recombinant BdTIR and AtTN7-TIR proteins and performed *in vitro* enzymatic activity assays on NAD+ using cADPR as a standard and BdTIR as a positive control. LC–MS results confirmed

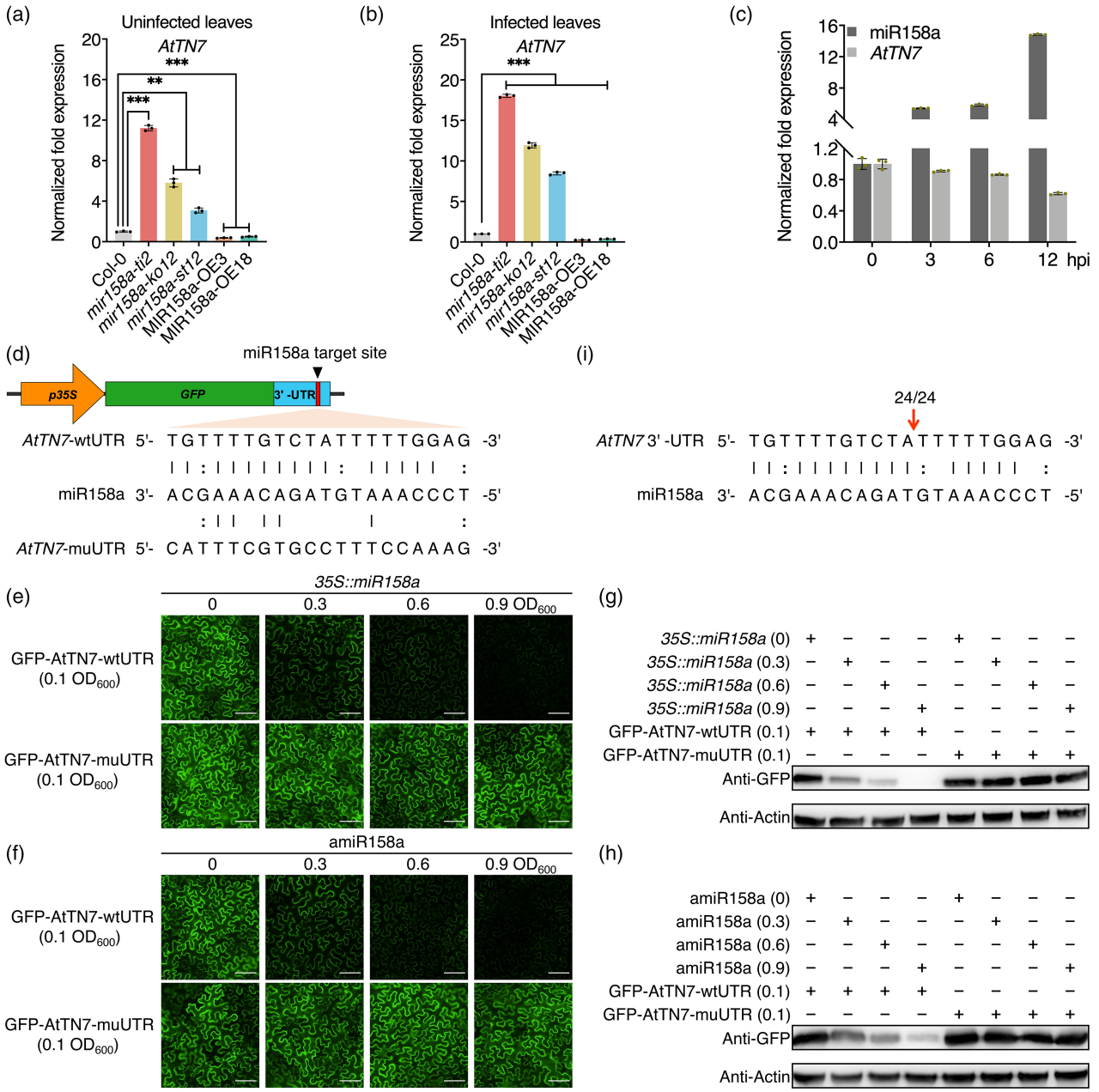

Figure 2. miR158a represses the expression of *AtTN7*.

(a) Relative expression level of *AtTN7* in *mir158a* mutants and MIR158a-OE lines uninfected with *Phytophthora parasitica*. Results are shown as the mean ± SD ($n = 3$).

(b) Relative expression level of *AtTN7* in *mir158a* mutants and MIR158a-OE lines at 12 h post-inoculation (hpi) with *P. parasitica*. Results are shown as the mean ± SD ($n = 3$).

(c) The expression level of miR158a and *AtTN7* in *Arabidopsis thaliana* leaves infected with *P. parasitica*. Results are shown as the mean ± SD ($n = 3$).

(d) Alignment of miR158a sequence with the nucleotide sequences of wild-type 3′-UTR (wtUTR) and mutated 3′-UTR (muUTR) of *AtTN7*.

(e, f) *Agrobacterium tumefaciens* carrying *35S::GFP-AtTN7-wtUTR* or *35S::GFP-AtTN7-muUTR* were expressed alone or co-expressed with *35S::miR158a* (e) or amiR158a (f) in *Nicotiana benthamiana* leaves. Images were taken using an Olympus fluorescence microscope to show the fluorescence intensity of GFP-AtTN7-wtUTR and GFP-AtTN7-muUTR at the same exposure intensity. Scale bars: 100 μm.

(g, h) The protein levels of GFP were displayed by Western blotting with Actin as a loading control.

(i) Cleavage site of *AtTN7* mRNA was revealed by mapping cloned RLM-5′ RACE products using *P. parasitica*-infected *Col-0 leaves at 12 hpi. The red arrow indicates the cleavage position and proportions of clones mapping to the site. The statistical analysis of (a) and (b) was conducted with Student's* t*-test. Asterisks indicate significant differences (*$P < 0.01$, ***$P < 0.001$).*

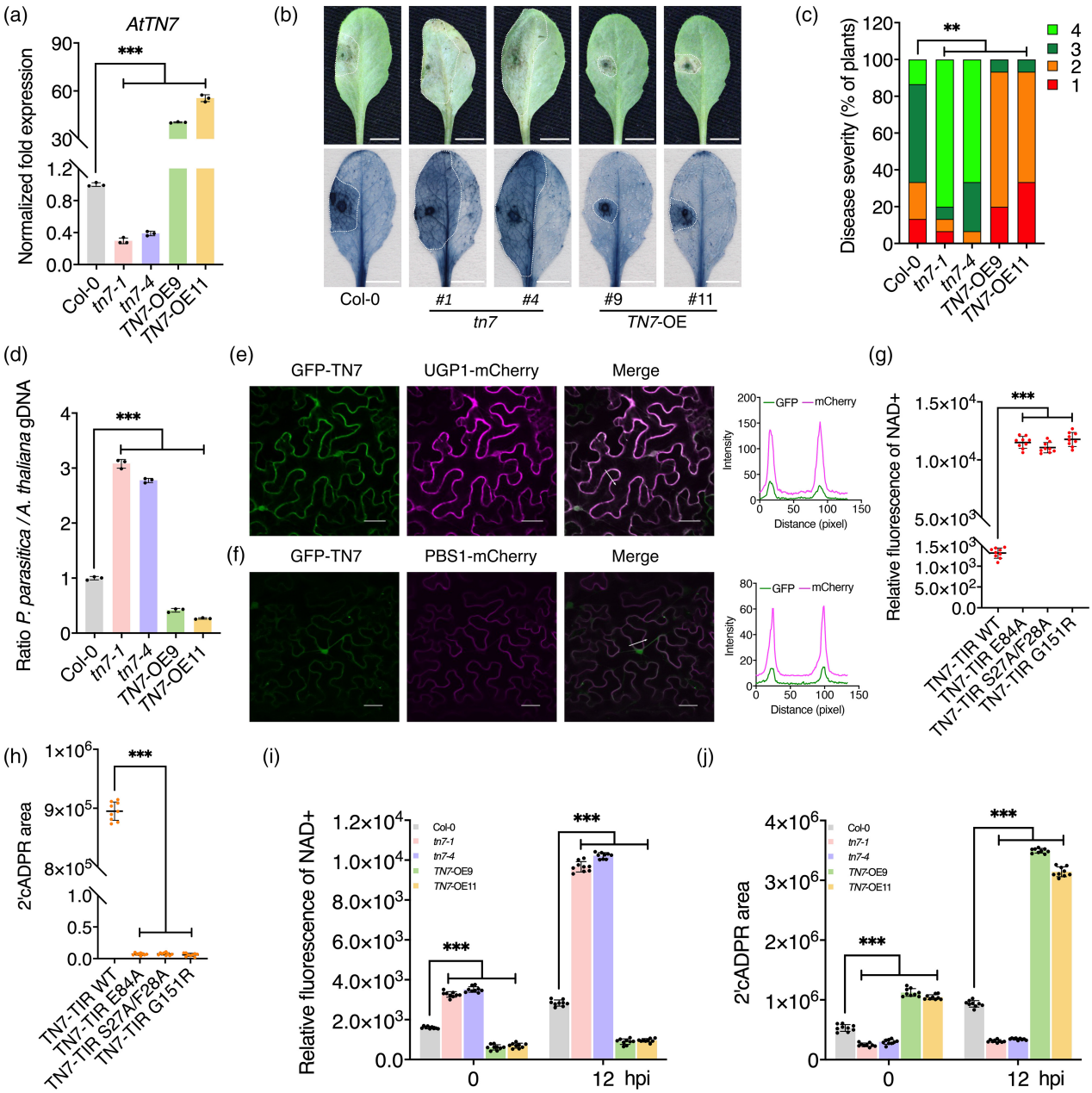

Figure 3. *AtTN7* positively regulates *Arabidopsis thaliana* resistance to *Phytophthora parasitica*.

(a) Relative expression level of *AtTN7* in *tn7* mutants and *TN7*-OE lines. The expression level was determined by RT-qPCR, with *A. thaliana UBC9* (*AtUBC9*) as an internal reference. Results are shown as the mean ± SD (n = 3).

(b) The disease symptoms of *tn7* mutants and *TN7*-OE lines plants inoculated with *P. parasitica* zoospores at 3 days post-inoculation (dpi). The infected area was observed and stained with trypan blue. Scale bars: 5 mm.

(c) Statistical analysis of plant disease grades. The evaluation and statistical analysis of plant disease grades were performed as described in Figure 1(e).

(d) The *P. parasitica* biomass was determined by quantitative PCR (qPCR). Results are shown as the mean ± SD (n = 3).

(e, f) The GFP-TN7 protein was localized in the cytoplasm (e) and the plasma membrane (f). The subcellular localization of the fusion protein in *Nicotiana benthamiana* leaves was determined using Olympus FV3000 confocal microscope at 3 days post Agroinfiltration. UGP1-mCherry was used as a cytoplasm marker. PBS1-mCherry was used as a plasma membrane marker. Scale bars: 40 μm.

(g, h) *In vitro* transcription-translation-generated AtTN7-TIR proteins drive NAD+ depletion. The contents of NAD+ (g) and 2′cADPR (h) in the reaction system were quantified. For example, "E84A" indicates a change at residue 84 from glutamic acid to alanine. Results are shown as the mean ± SD (n = 9).

(i, j) Plant NAD+ (i) and 2′cADPR (j) accumulations in *P. parasitica*-inoculated *leaves of* tn7 *mutants and* TN7-*OE lines at 0 and 12 h post-inoculation (hpi). Results are shown as the mean ± SD (*n* = *9). The statistical significance of (a, d) and (g–j) was assessed by Student's* t*-test. Asterisks indicate significant differences (**P < 0.01, ***P < 0.001).*

that the TIR domain of AtTN7 mainly produced 2′cADPR (Figure S9). To demonstrate the intrinsic enzymatic activity of AtTN7 TIR domain, we purified AtTN7-TIR (TN7-TIR WT) and AtTN7-TIR with the conserved amino acids mutation (TN7-TIR E84A, glutamic acid to alanine; TN7-TIR S27A/F28A, serine and phenylalanine to alanines; TN7-TIR G151R, glycine to arginine) after *in vitro* transcription-translation (Figures S10 and S11) and tested their ability to degrade NAD+ and produce 2′cADPR. NAD+ consumption and 2′cADPR accumulation occurred in TN7-TIR WT but not in the TN7-TIR E84A, TN7-TIR S27A/F28A, or TN7-TIR G151R treatments (Figure 3g,h).

To further validate AtTN7 functionality as a NADase *in planta*, we measured the content of NAD+ and 2′cADPR in plants. The NAD+ content was significantly higher in *tn7* mutants but lower in *TN7*-OE lines than that in Col-0 at both 0 and 12 hpi with *P. parasitica* (Figure 3i), while the content changes of 2′cADPR showed the opposite results (Figure 3j). We further observed that the elevated NAD+ and reduced 2′cADPR in *tn7-4* were recovered in *TN7*-CP lines, showing similar levels to those of Col-0 (Figure S12). These results suggested that AtTN7 had NAD+ cleavage activity and that its enzymatic activity relied on these conserved elements.

hNLR complex EDS1-PAD4-ADR1 is required for *TN7*-OE11- and *mir158a-ti2*-directed resistance to *P. parasitica*

Two different types of hNLRs complexes, EDS1-PAD4-ADR1 and EDS1-SAG101-NRG1 were reported to selectively convert TIR enzymatic activity into plant immune signals (Huang et al., 2022; Jacob et al., 2021; Jia et al., 2022; Sun et al., 2021). To examine whether they played a role in the immune responses of *TN7*-OE lines and *mir158a* mutants, we first quantified the transcript levels of *ADR1s* (*ADR1*, *ADR1-L1*, and *ADR1-L2*), *NRG1s* (*NRG1A*, *NRG1B*, and *NRG1C*), *EDS1*, *PAD4*, and *SAG101* in *TN7*-OE lines and *mir158a* mutants at 12 hpi with *P. parasitica*. The transcript levels of *ADR1s*, *EDS1*, and *PAD4* were significantly upregulated (Figure 4a,c), while the transcript levels of *NRG1s* and *SAG101* were downregulated or showed no significant differences (Figure 4b,c) in *TN7*-OE lines and *mir158a* mutants compared to Col-0.

To further analyze whether EDS1-PAD4-ADR1 or EDS1-SAG101-NRG1 complex was critical for the enhanced resistance of *TN7*-OE lines and *mir158a* mutants, we obtained and examined T-DNA insertion mutants (*adr1-L2*, SALK_076159C; *nrg1A*, SALK_101572C; *nrg1B*, SALK_020974C; *eds1-1*, SALK_152132C; *eds1-2*, SALK_017710C; *sag101-1*, SALK_022911C; *sag101-2*, SALK_030411C). The insertion sites of these mutants are shown in Figures S13–S17. We further generated triple mutants of *adr1s* and *nrg1s*, as well as knockout mutants of *eds1*, *pad4*, and *sag101* in both *TN7*-OE11 and *mir158a-ti2* background, using cross-hybridization and CRISPR/Cas9 editing approaches (Figures S18–S21). RT-qPCR analysis exhibited that the expression levels of *ADR1s*, *NRG1s*, *EDS1*, *PAD4*, and *SAG101* were significantly downregulated in these mutants (Figures S22–S24).

Infection assays showed that *TN7*-OE11/*adr1-5 adr1-L1/L2-2*, *TN7*-OE11/*adr1-6 adr1-L1/L2-2*, *TN7*-OE11/*eds1-7*, *TN7*-OE11/*eds1-9*, *TN7*-OE11/*pad4-4*, and *TN7*-OE11/*pad4-8* developed larger lesions and more *P. parasitica* biomass compared to *TN7*-OE11 plants (Figure 4d,f,g). However, *TN7*-OE11/*nrg1C-2 nrg1A/B-1*, *TN7*-OE11/*nrg1C-9 nrg1A/B-1*, *TN7*-OE11/*sag101-2*, and *TN7*-OE11/*sag101-6* showed no significant differences from *TN7*-OE11 plants (Figure 4d,f,g). Infection assays also revealed that *mir158a-ti2/adr1-1 adr1-L1/L2-2*, *mir158a-ti2/adr1-4 adr1-L1/L2-2*, *mir158a-ti2/eds1-3*, *mir158a-ti2/eds1-7*, *mir158a-ti2/pad4-6*, and *mir158a-ti2/pad4-9* showed enhanced susceptibility to *P. parasitica* compared to *mir158a-ti2* plants, as indicated by increased disease severity and more *P. parasitica* colonization (Figure 4e–g). However, no significant differences were detected between *mir158a-ti2/nrg1C-7 nrg1A/B-1*, *mir158a-ti2/nrg1C-8 nrg1A/B-1*, *mir158a-ti2/sag101-3*, or *mir158a-ti2/sag101-4* and *mir158a-ti2* (Figure 4e–g). These results suggested that EDS1-PAD4-ADR1 complex, but not EDS1-SAG101-NRG1 complex, was required not only for transduction of NADase activity signals of AtTN7 but also for the enhanced resistance of *TN7*-OE lines and *mir158a* mutants to *P. parasitica*.

AtTN7 promotes ADR1s-dependent Ca^{2+} influx to activate SA signaling

Prior researches suggest that the hNLRs can regulate intracellular Ca^{2+} concentration by forming influx channel (Essuman et al., 2022; Fliegert et al., 2007; Jacob et al., 2021). We observed elevated Ca^{2+} concentration in *TN7*-OE lines compared to Col-0 at 0 and 12 hpi with *P. parasitica* (Figure 5a), and the decreased Ca^{2+} in *tn7-4* was restored in *TN7*-CP lines (Figure S25a). To further confirm whether ADR1s mediated increased Ca^{2+} in *TN7*-OE lines, we quantified Ca^{2+} and found significantly decreased Ca^{2+} concentration in *TN7*-OE11/*adr1-5 adr1-L1/L2-2* and *TN7*-OE11/*adr1-6 adr1-L1/L2-2* plants compared to *TN7*-OE11 at 12 hpi with *P. parasitica* (Figure 5b), indicating that the AtTN7-induced increase in intracellular Ca^{2+} concentration was dependent on ADR1s.

Some *TN* genes function in SA-mediated defense responses (Nandety et al., 2013). We found that SA treatment increased the transcript level of *AtTN7* (Figure 5c), thus we speculated that AtTN7 may be involved in SA signaling. The expression levels of *PR1* and *CBP60g* were notably lower in *tn7* mutants, significantly higher in *TN7*-OE lines, but no difference from *TN7*-CP lines, compared to Col-0 at 12 hpi with *P. parasitica* (Figure 5d; Figure S25b). ADR1s contributed to enhanced resistance and induced Ca^{2+} influx in *TN7*-OE lines (Figures 4 and 5b).

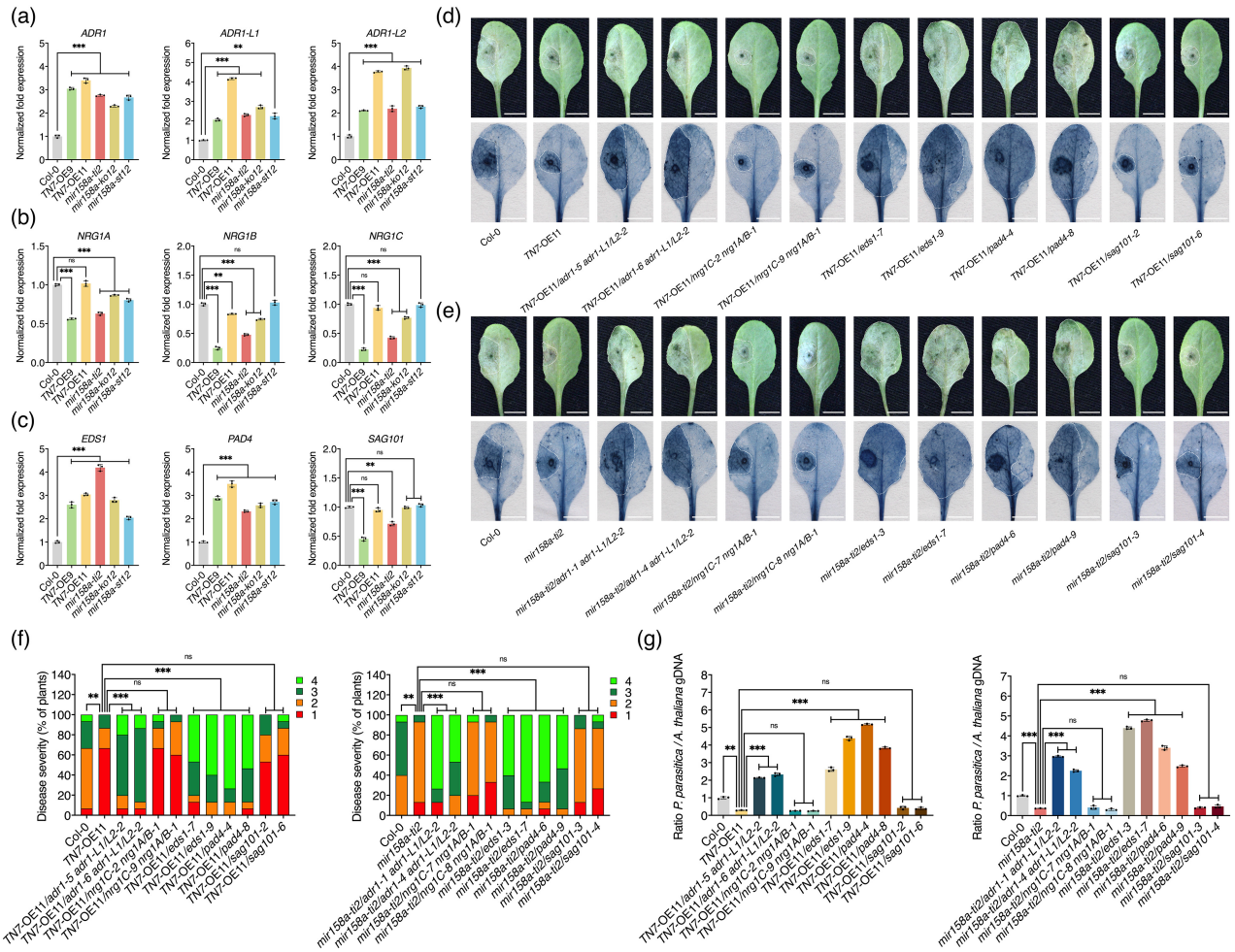

Figure 4. EDS1-PAD4-ADR1 complex is required for the enhanced resistance of *Arabidopsis thaliana TN7*-OE11 *and* mir158a-ti2 *plants to* Phytophthora parasitica.

(a–c) Relative expression levels of *ADR1s* (*ADR1*, *ADR1-L1*, *ADR1-L2*) (a), *NRG1s* (*NRG1A*, *NRG1B*, *NRG1C*) (b), *EDS1* (c), *PAD4* (c), and *SAG101* (c) in *TN7*-OE lines and *mir158a* mutants at 12 h post-inoculation (hpi) with *P. parasitica*. Results are shown as the mean ± SD (n = 3).

(d) Disease lesions of *TN7*-OE11, *TN7*-OE11/*adr1-5 adr1-L1/L2-2*, *TN7*-OE11/*adr1-6 adr1-L1/L2-2*, *TN7*-OE11/*nrg1C-2 nrg1A/B-1*, *TN7*-OE11/*nrg1C-9 nrg1A/B-1*, *TN7*-OE11/*eds1-7*, *TN7*-OE11/*eds1-9*, *TN7*-OE11/*pad4-4*, *TN7*-OE11/*pad4-8*, *TN7*-OE11/*sag101-2*, *TN7*-OE11/*sag101-6*, and Col-0 plants infected with *P. parasitica* zoospores at 3 days post-inoculation (dpi). The water-soaked lesions were colored by trypan blue staining. Scale bars: 5 mm.

(e) The disease symptoms of *mir158a-ti2*, *mir158a-ti2/adr1-1 adr1-L1/L2-2*, *mir158a-ti2/adr1-4 adr1-L1/L2-2*, *mir158a-ti2/nrg1C-7 nrg1A/B-1*, *mir158a-ti2/nrg1C-8 nrg1A/B-1*, *mir158a-ti2/eds1-3*, *mir158a-ti2/eds1-7*, *mir158a-ti2/pad4-6*, *mir158a-ti2/pad4-9*, *mir158a-ti2/sag101-3*, *mir158a-ti2/sag101-4*, and Col-0 plants inoculated with *P. parasitica* zoospores at 3 dpi. The infected area was observed and stained with trypan blue at 3 dpi. Scale bars: 5 mm.

(f) Statistical analysis of plant disease grades. The evaluation and statistical analysis of plant disease grades were performed as described in Figure 1(e).

(g) The *P. parasitica* colonization in infected leaves was measured by quantitative PCR (qPCR). Results are shown as the mean ± SD (n = 3). The statistical analysis of (a–c) and (g) was conducted with Student's t-test. Asterisks indicate significant differences (**P < 0.01, ***P < 0.001; ns, no significance).

We thus further proposed that ADR1s may be associated with AtTN7-activated SA signaling. We detected expression levels of *PR1* and *CBP60g* and found their obviously downregulation in *TN7*-OE11/*adr1-5 adr1-L1/L2-2* and *TN7*-OE11/*adr1-6 adr1-L1/L2-2* compared to *TN7*-OE11 plants at 12 hpi with *P. parasitica* (Figure 5e), implying that AtTN7-activated SA signaling required ADR1s function.

ADR1s are critical for both AtTN7-triggered Ca^{2+} influx and AtTN7-activated SA signaling (Figure 5b,e). Lanthanum (III) chloride ($LaCl_3$) is known to be a Ca^{2+} channel blocker, inhibiting Ca^{2+} influx into the cell (Kolodziej et al., 2021). We treated *A. thaliana* leaves with $LaCl_3$ and then inoculated them with *P. parasitica*, with water serving as a control. *TN7*-OE lines showed significantly decreased Ca^{2+} concentration after treatment with $LaCl_3$ as compared to Col-0 at 12 hpi (Figure 5f). We also found that the expression of *PR1* and *CBP60g* was notably downregulated in $LaCl_3$-treated *TN7*-OE lines at 12 hpi (Figure 5g). These data illustrated that ADR1s were indispensable for AtTN7-directed Ca^{2+} influx and SA signaling, and that activated SA signaling relied on Ca^{2+} influx to increase plant resistance to *P. parasitica*.

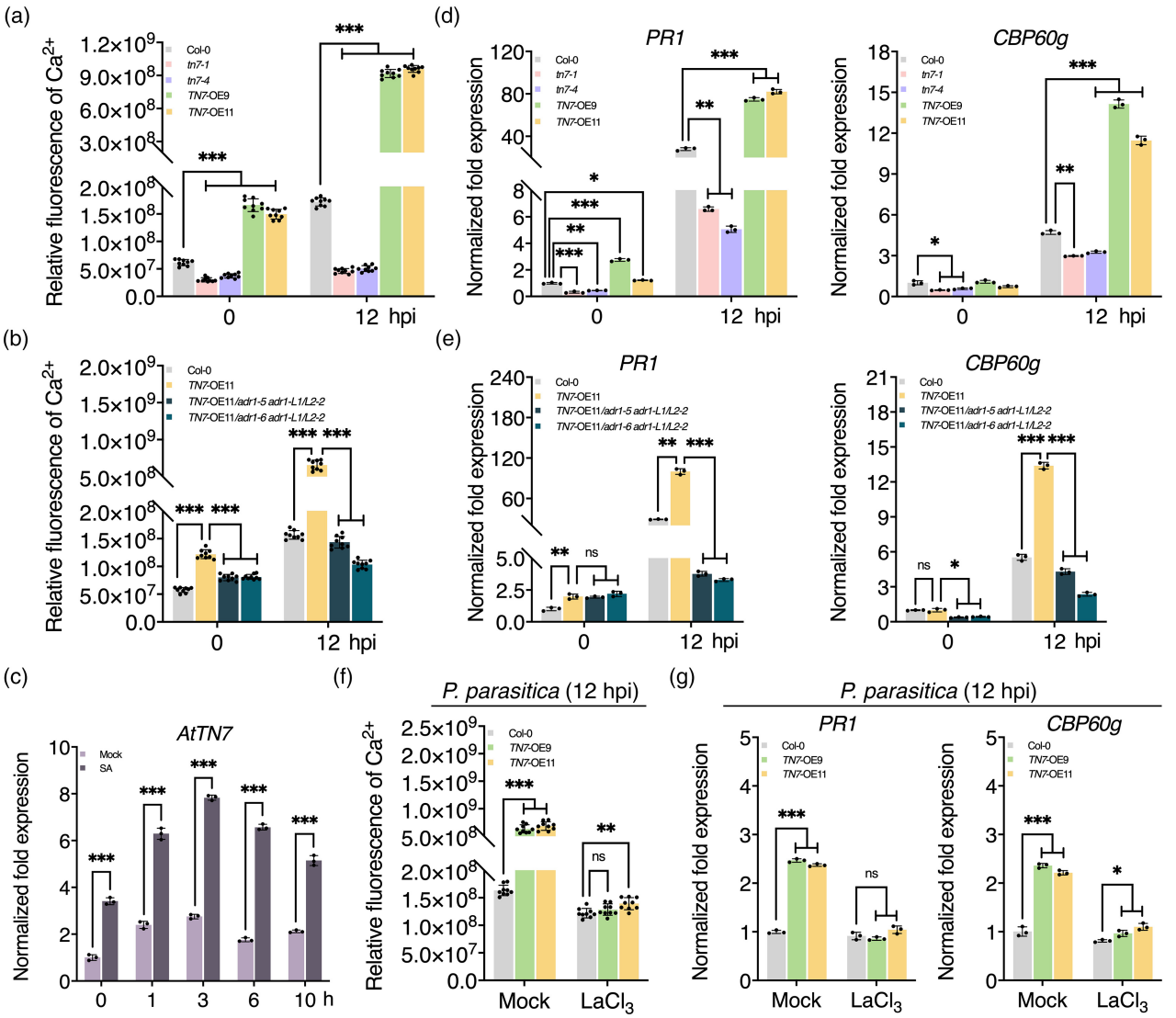

Figure 5. ADR1s-dependent Ca^{2+} influx activates SA signaling in *AtTN7* overexpression plants.
(a, b) The relative fluorescence of intracellular Ca^{2+} in *tn7* mutants (a), *TN7*-OE lines (a), *TN7*-OE11/*adr1-5 adr1-L1/L2-2* (b), *TN7*-OE11/*adr1-6 adr1-L1/L2-2* (b) and *TN7*-OE11 (b) at 0 and 12 h post-inoculation (hpi) with *Phytophthora parasitica*. Results are shown as the mean ± SD (n = 9).
(c) Expression level of *AtTN7* in *Arabidopsis thaliana* leaves at different time points after SA treatment. Results are shown as the mean ± SD (n = 3).
(d, e) Relative expression levels of *PR1* and *CBP60g* in *tn7* mutants (d), *TN7*-OE lines (d), *TN7*-OE11/*adr1-5 adr1-L1/L2-2* (e), *TN7*-OE11/*adr1-6 adr1-L1/L2-2* (e) and *TN7*-OE11 (e) at 0 and 12 hpi with *P. parasitica*. Results are shown as the mean ± SD (n = 3).
(f) The leaves of 4-week-old *TN7*-OE lines and Col-0 plants were treated with 1 mM $LaCl_3$ or with water as a control treatment. The relative fluorescence of intracellular Ca^{2+} was measured at 12 hpi with *P. parasitica*. Results are shown as the mean ± SD (n = 9).
(g) Expression levels of *PR1* and *CBP60g* in *TN7*-OE lines and Col-0 leaves treated with $LaCl_3$ and inoculated with *P. parasitica* for 12 h. Results are shown as the mean ± SD (n = 3). The statistical significance of (a–g) was assessed by Student's t-test. Asterisks indicate significant differences (*P < 0.05, **P < 0.01, ***P < 0.001; ns, no significance).

miR158a suppresses AtTN7-triggered plant resistance to *P. parasitica*

Since miR158a repressed expression of *AtTN7*, we further examined whether miR158a-mediated *AtTN7* downregulation inhibited AtTN7-activated plant resistance. To verify whether miR158a affected the NADase activity of AtTN7, we quantified NAD+ and 2′cADPR content in leaves of *mir158a* mutants, MIR158a-OE lines, and Col-0 at 0 and 12 hpi with *P. parasitica*. The *mir158a* mutants had less NAD+ and more 2′cADPR, while the MIR158a-OE lines had more NAD+ and less 2′cADPR than Col-0 (Figure 6a,b), suggesting that the NADase activity of AtTN7 was repressed by miR158a.

mir158a mutants relied on the hNLR EDS1-PAD4-ADR1 complex to increase resistance to *P. parasitica* (Figure 4e–g). To investigate whether *mir158a* mutants

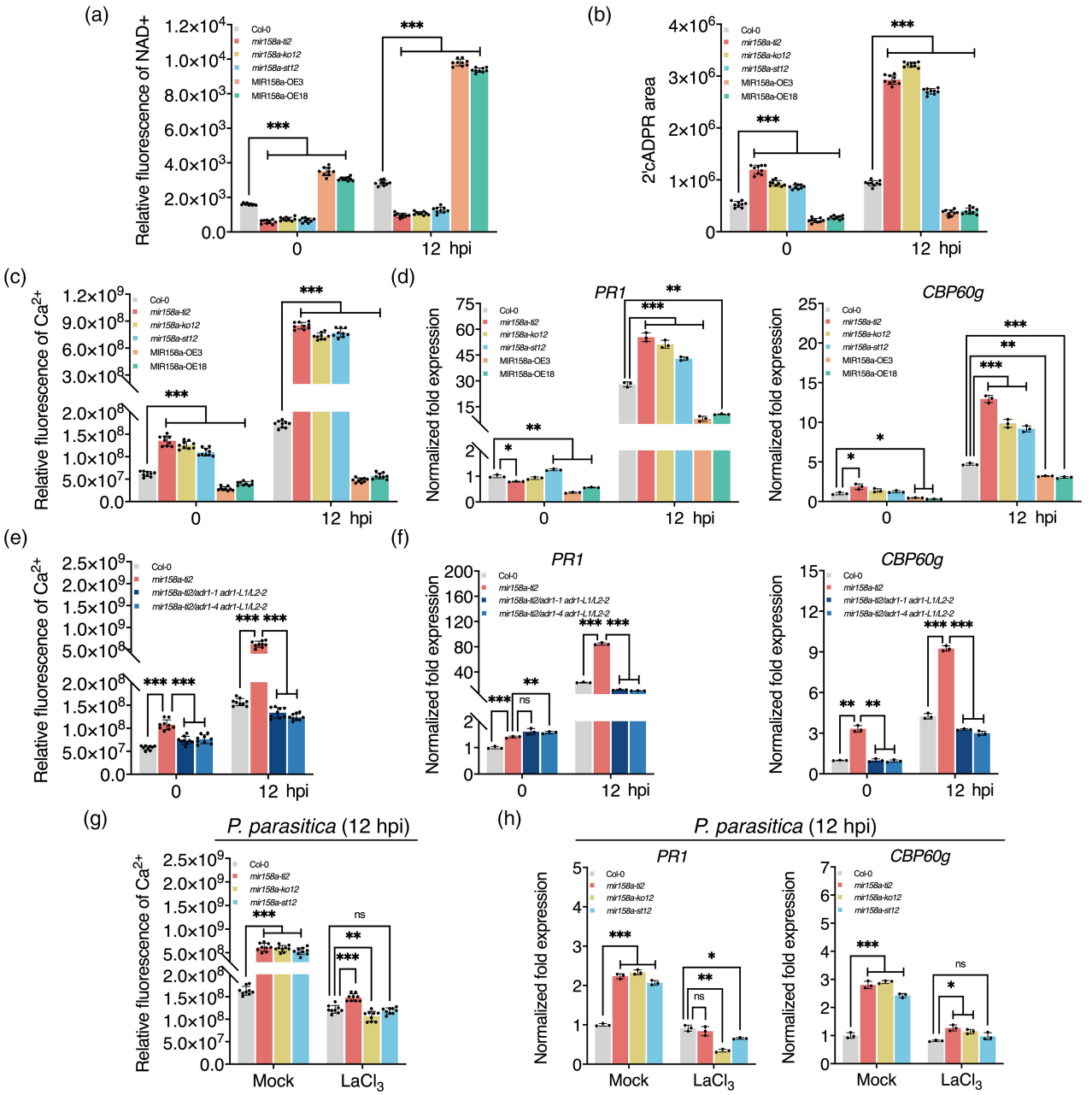

Figure 6. miR158a negatively regulates AtTN7-mediated *Arabidopsis thaliana* immunity to *Phytophthora parasitica*.
(a, b) The NAD+ accumulation (a) and 2′cADPR content (b) in the leaves of *mir158a* mutants and MIR158a-OE lines at 0 and 12 h after *P. parasitica* infection. Results are shown as the mean ± SD (n = 9).
(c, e) The relative fluorescence of intracellular Ca^{2+} in *mir158a* mutants (c), MIR158a-OE lines (c), *mir158a-ti2/adr1-1 adr1-L1/L2-2* (e), *mir158a-ti2/adr1-4 adr1-L1/L2-2* (e), and *mir158a-ti2* (e) at 0 and 12 h post-inoculation (hpi) with *P. parasitica*. Results are shown as the mean ± SD (n = 9).
(d, f) Relative expression levels of *PR1* and *CBP60g* in *mir158a* mutants (d), MIR158a-OE lines (d), *mir158a-ti2/adr1-1 adr1-L1/L2-2* (f), *mir158a-ti2/adr1-4 adr1-L1/L2-2* (f), and *mir158a-ti2* (f) at 0 and 12 h after *P. parasitica* infection. Results are shown as the mean ± SD (n = 3).
(g) The relative fluorescence of intracellular Ca^{2+} in 1 mM $LaCl_3$-treated *mir158a* mutants and Col-0 leaves were measured at 12 hpi with *P. parasitica*. Water as a control treatment. Results are shown as the mean ± SD (n = 9).
(h) Expression levels of *PR1* and *CBP60g* in *mir158a* mutants and Col-0 leaves treated with $LaCl_3$ and inoculated with *P. parasitica* for 12 h. Results are shown as the mean ± SD (n = 3). The statistical significance of (a–h) was assessed by Student's t-test. Asterisks indicate significant differences (*P < 0.05, **P < 0.01, ***P < 0.001; ns, no significance).

promote ADR1s-dependent Ca^{2+} influx, we quantified intracellular Ca^{2+} concentration derived from leaves inoculated with *P. parasitica*. Ca^{2+} concentrations were elevated in *mir158a* mutants but significantly lower in MIR158a-OE lines compared to Col-0 across infection stages (Figure 6c), and the Ca^{2+} elevation was abolished in *mir158a-ti2/adr1-1*

adr1-L1/L2-2 and *mir158a-ti2/adr1-4 adr1-L1/L2-2* at 12 hpi with *P. parasitica* (Figure 6e), indicating that miR158a inhibited AtTN7-triggered ADR1s-dependent Ca^{2+} influx.

To confirm whether miR158a could restrict SA signaling activated by ADR1s-dependent Ca^{2+} influx, we first measured the expression levels of *PR1* and *CBP60g* in *P. parasitica*-infected leaves. We found that *PR1* and *CBP60g* expression was upregulated in *mir158a* mutants but downregulated in MIR158a-OE lines compared to Col-0 at 12 hpi (Figure 6d), and the increased expression of *PR1* and *CBP60g* in *mir158a-ti2* disappeared in *mir158a-ti2/adr1-1 adr1-L1/L2-2* and *mir158a-ti2/adr1-4 adr1-L1/L2-2* at 12 hpi (Figure 6f). Next, we treated leaves with $LaCl_3$. We found that when treated with $LaCl_3$, *mir158a* mutants showed reduced Ca^{2+} concentration compared to Col-0 at 12 hpi with *P. parasitica* (Figure 6g), and the expression of *PR1* and *CBP60g* in $LaCl_3$-treated *mir158a* mutants was lower than those of Col-0 at 12 hpi (Figure 6h). These results confirmed that miR158a negatively regulated plant immunity by repressing *AtTN7* transcripts, resulting in the suppressed AtTN7 NADase activity and activation of hNLR EDS1-PAD4-ADR1 complex, leading to interfered ADR1s-dependent Ca^{2+} influx-induced SA immune signaling.

DISCUSSION

miRNAs are important regulators in plant innate immunity, including understanding of plant susceptibility to oomycete pathogens (Brant & Budak, 2018; Fei et al., 2016; Gou et al., 2022; López-Márquez et al., 2023). Previous studies have shown that miR158 functions in *B. campestris* pollen development (Ma et al., 2017), *I. batatas* abiotic stress response (Sun et al., 2022), and *A. thaliana* adaptation (Tripathi et al., 2023). Here, we identified that *A. thaliana* miR158a has differential expression levels in leaf following *P. parasitica* infection and is selected for functional analysis (Figure S1). We show that miR158a plays a negative regulatory role in the immune responses of *A. thaliana* against *P. parasitica* (Figure 1), indicating the functional diversity and complexity of plant miR158.

Our results demonstrate that *AtTN7* is an authentic target of miR158a, and its downregulation by miR158a is achieved by cleaving 3′-UTR of *AtTN7* (Figure 2; Figure S2). We confirm that *AtTN7* acts as a positive regulator of plant immunity to *P. parasitica* (Figure 3a–d). *AtTN7* encodes a TIR-NBS protein (Figure S5). Plant TIR domains have NAD+ cleavage activity, and several conserved amino acids affect TIR-mediated NAD+ hydrolytic activity (Lapin et al., 2022; Wan et al., 2019). The latest research shows that when the expression of TIR-domain disease resistance gene is upregulated or induced by pathogen, its NAD+ hydrolase activity can be activated to produce immune signaling molecules (Song et al., 2024). The TIR domain of AtTN7 could homodimerize and has conserved amino acid residues required for NAD+ degradation (Figures S5 and S8), but whether AtTN7 acts as a NAD+ cleavage enzyme remains unknown. In this study, we illustrate that the TIR domain of AtTN7 has the ability to consume NAD+ to produce 2′cADPR (Figure S9), and the NADase activity is dependent on the conserved amino acids (Figure 3g–j). TIR-mediated immune responses in *A. thaliana* are reported to depend on EDS1-PAD4-ADR1 or EDS1-SAG101-NRG1 complex to convert NADase activity signals into immune signals (Castel et al., 2019; Huang et al., 2022; Lapin et al., 2022). Our findings reveal that EDS1-PAD4-ADR1 complex, but not EDS1-SAG101-NRG1 complex, participates in plant resistance in *AtTN7*-overexpressing plants-triggered resistance to *P. parasitica* (Figure 4). The enzymatic activity signals generated by NAD+ degradation by AtTN7 are converted into immune signals through EDS1-PAD4-ADR1 complex, which promotes AtTN7-mediated plant resistance to *P. parasitica*. Our study reveals the importance and complexity of *AtTN7* in regulating plant basal immunity, which expands our understanding of the function of *TN* genes in plant immunity. In addition, similar to *AtTN7*, *AtTN2* also relies on downstream ADR1s to exert its immune function (Wang et al., 2021). Interestingly, AtTN2 induces cell death (Wang et al., 2021), while AtTN7 triggers basal resistance. Further investigation of why these two different immune phenotypes occur will be useful to gain a deeper understanding of the mechanism by which *TN* genes regulate plant immunity.

Furthermore, how EDS1-PAD4-ADR1 complex regulates AtTN7-mediated basal resistance is largely unknown. In this study, we found that AtTN7-triggered Ca^{2+} influx and SA signaling are both dependent on ADR1s (Figure 5a–e). Further exploration shows that the activation of SA signaling relies on Ca^{2+} influx (Figure 5f,g). Our results manifest that the NAD+ cleavage products of AtTN7 activate Ca^{2+} influx by integrating with EDS1-PAD4-ADR1 complex, and ADR1s-dependent Ca^{2+} influx promotes AtTN7-induced plant resistance through the activation of SA signaling. Moreover, the ability of *AtTN7* complementation lines to restore the phenotypes to wild-type levels also strongly supports our findings on the mechanism of *AtTN7* regulating plant immunity (Figures S4, S12, and S25). Our work basically explains the mechanism of how *AtTN7* enhances *A. thaliana* resistance to *P. parasitica*. Previous studies have shown that Ca^{2+} signaling and SA signaling may influence each other (Cui, Gobbato, et al., 2017; Du et al., 2009; Lapin et al., 2022; Sun et al., 2015; Zhang & Li, 2019). It will be interesting to further clarify how ADR1s-dependent Ca^{2+} influx regulates SA signaling and whether it regulates other signaling to promote AtTN7-mediated plant immunity.

miR173 triggers the production of tasiRNAs at the TAS1/2 sites (Felippes & Weigel, 2009; Yoshikawa et al., 2016), some of which are predicted to target the *PPR* genes to produce phasiRNAs (Howell et al., 2007; Xia et al., 2013). This miRNA–*TASL*–*PPR*–siRNA pathway has

been reported to be conserved in many plant species (Tripathi et al., 2023; Xia et al., 2013). Silencing of miR158a results in increased expression of its target gene pseudo-*PPR*. Pseudo-*PPR* transcripts can be targeted by two miR173-mediated tasiRNAs (siR9 and siR12) from the TAS2 locus, leading to biogenesis of phasiRNAs. One of the phasiRNAs generated by this mechanism degrades the *NHX2* transcripts to regulate stomatal function (Tripathi et al., 2023). The above evidence indicates that the deletion of miR158a could induce production of miR173-mediated phasiRNAs to regulate plant growth and development. Therefore, some phasiRNAs may target other RNL transcripts to amplify the impact on basal immunity, which deserves further investigation.

In conclusion, our study reveals the immune roles and regulatory mechanisms of miR158a and *AtTN7*. miR158a attenuates *A. thaliana* resistance to *P. parasitica* by suppressing the expression of *AtTN7* (Figure 7). AtTN7-mediated resistance is dependent on its NADase activity and EDS1-PAD4-ADR1 complex. Furthermore, ADR1s-dependent Ca^{2+} influx-activated SA signaling is involved in the AtTN7-mediated plant resistance. In addition, both downregulation of miR158a and overexpression of *AtTN7* lead to enhanced plant resistance to *P. parasitica* without affecting plant growth phenotypes (Figure S26), suggesting their application potentials in crop disease resistance breeding. The identification and utilization of miRNAs and their target genes involved in plant susceptibility provide an efficient approach for the development of plant germplasm resources with durable resistance.

EXPERIMENTAL PROCEDURES

Plant materials and growth conditions

Arabidopsis thaliana and *Nicotiana benthamiana* plants were grown in a controlled environmental growth room at 23 ± 1°C in a 12 h light/12 h dark photoperiod. All experiments were performed on 4-week-old plants. The *A. thaliana* T-DNA insertion mutants were purchased from AraShare (https://www.arashare.cn/index/). *A. thaliana* Col-0 served as the wild-type in this study. All *A. thaliana* transgenic lines except the *AtTN7* complementation transgenic lines were prepared in the Col-0 background. The *AtTN7* complementation transgenic lines were generated in the *tn7-4* background. All *A. thaliana* transgenic lines were prepared by the *Agrobacterium tumefaciens*-mediated transformation (Zhang et al., 2006). These lines were identified by appropriate antibiotic selection and DNA sequencing analysis.

Plasmid construction

pART27 vector was used to prepare overexpressed and silenced transgenic plants, as well as plant transient expression. PKI1.1R vector was used to obtain knockout transgenic plants. pMDC32 vector was used to prepare complementation transgenic plants. DHFR vector was used in *in vitro* NADase assays. All primers used in this study are listed in Table S1. A complete description of plasmid construction is included in Methods S1.

Pathogen cultural conditions and inoculation

Phytophthora parasitica strain Pp016-GFP was used for infection assays. Pathogen culture and zoospores preparation were performed according to a previous study (Wang et al., 2011). The detached leaves at the same leaf position on 4-week-old *A. thaliana* were inoculated with 2×10^3 *P. parasitica* zoospores, then observed the fluorescence distribution of hyphae on the leaves under a fluorescence microscope to determine the lesion

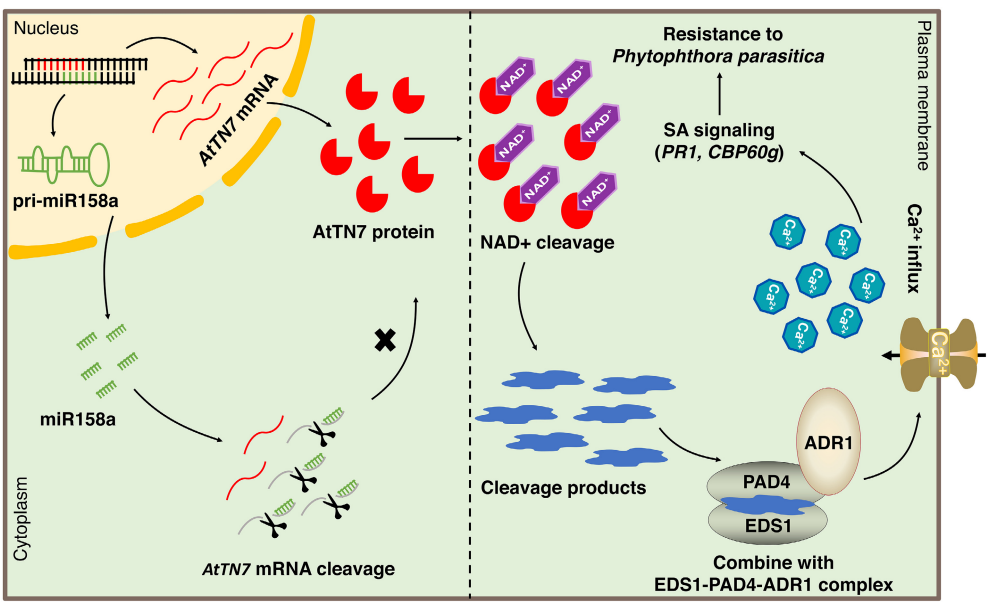

Figure 7. A model of miR158a represses AtTN7-triggered *Arabidopsis thaliana* resistance to *Phytophthora parasitica*.
During *P. parasitica* infection, AtTN7 relies on its NADase activity and EDS1-PAD4-ADR1 complex to activate plant immunity. Subsequently, ADR1s-dependent Ca^{2+} influx induces the downstream SA signaling, leading to enhanced *A. thaliana* resistance against *P. parasitica*. In this process, miR158a cleaves *AtTN7* mRNA to inhibit AtTN7-mediated resistance.

diameters at 3 dpi. At least 10 leaves for the inoculation assays. The inoculation assays were performed three times.

RNA extraction and RT-qPCR analysis

Using the RNAsimple Total RNA Kit (TIANGEN, Beijing, China) to extract total RNA from the whole leaves before and after *P. parasitica* inoculations. Using the Evo M-MLV RT Kit with gDNA Clean for qPCR (Accurate Biology, Changsha, China) to synthesize cDNA. Using UltraSYBR Mixture (CWBIO, Beijing, China) to prepare RT-qPCR reaction system. The RT-qPCR assays were set up with three biological replicates. Primers used for RT-qPCR analysis are listed in Table S1.

Transient expression assays

Agrobacterium tumefaciens was used to conduct transient expression assays in *N. benthamiana* leaves based on previous report (Huang et al., 2019). Detailed description of transient expression assays is in Methods S2.

Subcellular localization

Using the *A. tumefaciens*-mediated transient expression system of *N. benthamiana*, the fluorescent-tagged gene was transiently expressed for 3 days, and then fluorescence observation was performed and images were collected using Olympus FV3000 confocal microscope (Olympus, Tokyo, Japan). UGP1-mCherry (*AT3G03250*) was used as a cytoplasm marker, and PBS1-mCherry served as a plasma membrane marker (Qi et al., 2014).

RLM-5′ RACE of mRNA cleavage products

RLM-5′ RACE was performed to analyze the cleavage site of miR158a in *AtTN7*. The experimental procedures were based on the FirstChoice® RLM-RACE Kit (Invitrogen™, Carlsbad, CA, USA) with slight modifications. Briefly, the Evo M-MLV RT kit with gDNA Clean for qPCR (Accurate Biology, Changsha, China) was used to remove the gDNA of the total RNA extracted from *P. parasitica*-infected *A. thaliana* leaves at 12 hpi, and then the 5′ RACE adapter was directly ligated to the degraded mRNA using T4 RNA ligase. Oligo dT (18 T) was used for reverse transcription to synthesize cDNA. The target fragment amplified by nested PCR was ligated into a pMD®19-T vector (TaKaRa, Kusatsu, Japan) for sequencing. The primers for nested PCR are listed in Table S1.

Cell-free transcription and translation

In vitro cell-free protein transcription and translation were performed using the PURExpress In Vitro Protein Synthesis Kit (New England BioLabs, Ipswich, MA, USA). Full description of cell-free transcription and translation is included in Methods S3.

Native protein purification

The cell-free synthesized proteins were purified as previously reported (Wan et al., 2019). A detailed description of native protein purification is included in Methods S4.

In vitro NADase assay with purified protein

NADase activity was measured as previously reported (Wan et al., 2019). Complete description of *in vitro* NADase assay with purified protein is included in Methods S5.

NAD+ measurement

NAD+ quantification was performed as previously reported (Bayless et al., 2023). The Amplite NAD+ Assay Kit (AAT Biosciences, Pleasanton, CA, USA) was used according to user manual with 96-well black bottom plates (Costar, Washington, USA). Full description of NAD+ measurement is included in Methods S6.

LC–MS analysis of 2′cADPR

LC–MS analysis was performed to identify and quantify 2′cADPR as previously reported (Bayless et al., 2023). The 2′cADPR was identified based on the retention time. The 2′cADPR content in different samples was quantified by peak area. Detailed description of 2′cADPR detection is included in Methods S7.

Ca^{2+} detection

Ca^{2+} quantification was performed with the Fluo-4 NW Calcium Assay Kits (Invitrogen) according to the user manual. Full description of Ca^{2+} content measurement is included in Methods S8.

Co-immunoprecipitation assays

Anti-GFP Nanobody Magarose Beads (AlpaLifeBio, Shenzhen, China) were used for the co-immunoprecipitation assays based on the user manual. Detailed description of co-immunoprecipitation assays is in Methods S9.

His pull-down assays

His affinity Cobalt (Co^{2+}) Dynabeads magnetic beads (Invitrogen) were used for the His pull-down assays according to the user manual. Full description of His pull-down assays is included in Methods S10.

Statistical analysis

Using Student's *t*-test to analyze the data of NAD+ fluorescence intensity, 2′cADPR content, Ca^{2+} fluorescence intensity, biomass and gene expression. Using Wilcoxon rank-sum test to analyze the data of plant disease grades. Asterisks indicate significant differences ($*P < 0.05$, $**P < 0.01$, $***P < 0.001$; ns, no significance).

ACCESSION NUMBERS

Accession numbers are as follows: AT3G10745 (*MIR158a*), AT1G72900 (*AtTN7*), AT1G33560 (*ADR1*), AT4G33300 (*ADR1-L1*), AT5G04720 (*ADR1-L2*), AT5G66900 (*NRG1A*), AT5G66910 (*NRG1B*), AT5G66890 (*NRG1C*), AT3G48090 (*EDS1*), AT3G52430 (*PAD4*), AT5G14930 (*SAG101*), AT2G14610 (*PR1*), AT5G26920 (*CBP60g*).

AUTHOR CONTRIBUTIONS

WS and YL designed the research. YL, XG, RM, and PZ performed the experiments. YL, AA, QS, ZL, and YM analyzed the data. YL and WS wrote the manuscript.

ACKNOWLEDGMENTS

We thank Professor Murray Grant (University Warwick, UK), Dr Yang Yang (Northwest A&F University, China) for their pertinent suggestions. We also thank Ms. Jian Liru and Ms. Li Xiuhuan (State Key Laboratory of Crop Stress Resistance and High-Efficiency Production) for their assistance in the experiments. This work was supported by the China Agriculture Research System (CARS-09), the National Natural Science Foundation of China

(#31125022), and the Program of Introducing Talents of Innovative Discipline to Universities (project 111) from the State Administration of Foreign Experts Affairs (#B18042).

CONFLICT OF INTEREST

The authors declare no competing interests.

DATA AVAILABILITY STATEMENT

The data that support the findings of this study are available from the corresponding author upon reasonable request.

SUPPORTING INFORMATION

Additional Supporting Information may be found in the online version of this article.

Figure S1. The expression pattern of miR158a during *Phytophthora parasitica* infection.

Figure S2. RLM-5′ RACE sequencing results of miR158a-mediated *AtTN7* mRNA cleavage site.

Figure S3. Schematic representation of the editing sites in the *AtTN7* CRISPR/Cas9 mutants.

Figure S4. *TN7*-CP lines were restored to the wild-type disease phenotypes upon *P. parasitica*.

Figure S5. AtTN7 protein sequence alignment.

Figure S6. The protein expression of GFP-TN7 and UGP1-mCherry.

Figure S7. The protein expression of GFP-TN7 and PBS1-mCherry.

Figure S8. The homodimerization of AtTN7 TIR domain.

Figure S9. AtTN7-TIR produces 2′cADPR as a major product.

Figure S10. Schematic diagram of amino acid mutations in AtTN7 TIR domain.

Figure S11. Detection of purified cell-free synthesized proteins.

Figure S12. The NAD+ and 2′cADPR contents in *TN7*-CP lines.

Figure S13. Schematic diagram of the T-DNA insertion site of *adr1-L2*.

Figure S14. Schematic diagram of the T-DNA insertion site of *nrg1A*.

Figure S15. Schematic diagram of the T-DNA insertion site of *nrg1B*.

Figure S16. Schematic diagram of the T-DNA insertion sites of *eds1-1* and *eds1-2*.

Figure S17. Schematic diagram of the T-DNA insertion sites of *sag101-1* and *sag101-2*.

Figure S18. Schematic representation of the editing sites in the *ADR1-L1* CRISPR/Cas9 mutant.

Figure S19. Schematic representation of the editing sites in the *ADR1* CRISPR/Cas9 mutants.

Figure S20. Schematic representation of the editing sites in the *NRG1C* CRISPR/Cas9 mutants.

Figure S21. Schematic representation of the editing sites in the *PAD4* CRISPR/Cas9 mutants.

Figure S22. The expression levels of *ADR1s* in mutants.

Figure S23. The expression levels of *NRG1s* in mutants.

Figure S24. The expression levels of *EDS1*, *PAD4*, and *SAG101* in mutants.

Figure S25. The Ca^{2+} content and transcript levels of *PR1* and *CBP60g* in *TN7*-CP lines.

Figure S26. The growth phenotypes of *mir158a* mutants, MIR158a-OE lines, *tn7* mutants, *TN7*-OE lines, and *TN7*-CP lines.

Table S1. Primers used in this study.

Methods S1. Plasmid construction.

Methods S2. Transient expression assays.

Methods S3. Cell-free transcription and translation.

Methods S4. Native protein purification.

Methods S5. *In vitro* NADase assay with purified protein.

Methods S6. NAD+ measurement.

Methods S7. LC–MS analysis of 2′cADPR.

Methods S8. Ca^{2+} detection.

Methods S9. Co-immunoprecipitation assays.

Methods S10. His pull-down assays.

REFERENCES

Avila-Quezada, G.D. & **Rai, M.** (2023) Novel nanotechnological approaches for managing *Phytophthora* diseases of plants. *Trends in Plant Science*, **28**, 1070–1080. Available from: https://doi.org/10.1016/j.tplants.2023.03.022

Bayless, A.M., **Chen, S.**, **Ogden, S.C.**, **Xu, X.**, **Sidda, J.D.**, **Manik, M.K.** ***et al.*** (2023) Plant and prokaryotic TIR domains generate distinct cyclic ADPR NADase products. *Science Advances*, **9**, eade8487. Available from: https://doi.org/10.1126/sciadv.ade8487

Brant, E.J. & **Budak, H.** (2018) Plant small non-coding RNAs and their roles in biotic stresses. *Frontiers in Plant Science*, **9**, 1038. Available from: https://doi.org/10.3389/fpls.2018.01038

Castel, B., **Ngou, P.-M.**, **Cevik, V.**, **Redkar, A.**, **Kim, D.-S.**, **Yang, Y.** ***et al.*** (2019) Diverse NLR immune receptors activate defence via the RPW8-NLR NRG1. *New Phytologist*, **222**, 966–980. Available from: https://doi.org/10.1111/nph.15659

Chen, Y., **Zhong, G.**, **Cai, H.**, **Chen, R.**, **Liu, N.**, **Wang, W.** ***et al.*** (2021) A truncated TIR-NBS protein TN10 pairs with two clustered TIR-NBS-LRR immune receptors and contributes to plant immunity in *Arabidopsis*. *International Journal of Molecular Sciences*, **22**, 4004. Available from: https://doi.org/10.3390/ijms22084004

Cui, H., **Gobbato, E.**, **Kracher, B.**, **Qiu, J.**, **Bautor, J.** & **Parker, J.E.** (2017) A core function of EDS1 with PAD4 is to protect the salicylic acid defense sector in *Arabidopsis* immunity. *New Phytologist*, **213**, 1802–1817. Available from: https://doi.org/10.1111/nph.14302

Cui, X., **Yan, Q.**, **Gan, S.**, **Xue, D.**, **Dou, D.**, **Guo, N.** ***et al.*** (2017) Overexpression of gma-miR1510a/b suppresses the expression of a NB-LRR domain gene and reduces resistance to *Phytophthora sojae*. *Gene*, **621**, 32–39. Available from: https://doi.org/10.1016/j.gene.2017.04.015

Dai, X. & **Zhao, P.X.** (2011) psRNATarget: a plant small RNA target analysis server. *Nucleic Acids Research*, **39**, W155–W199. Available from: https://doi.org/10.1093/nar/gkr319

Dongus, J.A. & **Parker, J.E.** (2021) EDS1 signalling: at the nexus of intracellular and surface receptor immunity. *Current Opinion in Plant Biology*, **62**, 102039. Available from: https://doi.org/10.1016/j.pbi.2021.102039

Du, L., **Ali, G.S.**, **Simons, K.A.**, **Hou, J.**, **Yang, T.**, **Reddy, A.S.N.** ***et al.*** (2009) Ca^{2+}/calmodulin regulates salicylic-acid-mediated plant immunity. *Nature*, **457**, 1154–1158. Available from: https://doi.org/10.1038/nature07612

Duxbury, Z., **Wang, S.**, **MacKenzie, C.I.**, **Tenthorey, J.L.**, **Zhang, X.**, **Huh, S.U.** ***et al.*** (2020) Induced proximity of a TIR signaling domain on a plant-mammalian NLR chimera activates defense in plants. *Proceedings of the National Academy of Sciences of the United States of America*, **117**, 18832–18839. Available from: https://doi.org/10.1073/pnas.2001185117

Essuman, K., **Milbrandt, J.**, **Dangl, J.L.** & **Nishimura, M.T.** (2022) Shared TIR enzymatic functions regulate cell death and immunity across the tree of life. *Science*, **377**, eabo0001. Available from: https://doi.org/10.1126/science.abo0001

Fahlgren, N., **Howell, M.D.**, **Kasschau, K.D.**, **Chapman, E.J.**, **Sullivan, C.M.**, **Cumbie, J.S.** ***et al.*** (2007) High-throughput sequencing of *Arabidopsis* microRNAs: evidence for frequent birth and death of MIRNA genes. *PLoS One*, **2**, e219. Available from: https://doi.org/10.1371/journal.pone.0000219

Feehan, J.M., **Castel, B.**, **Bentham, A.R.** & **Jones, J.D.G.** (2020) Plant NLRs get by with a little help from their friends. *Current Opinion in Plant Biology*, **56**, 99–108. Available from: https://doi.org/10.1016/j.pbi.2020.04.006

Fei, Q., **Zhang, Y.**, **Xia, R.** & **Meyers, B.C.** (2016) Small RNAs add zing to the zig-zag-zig model of plant defenses. *Molecular Plant-Microbe Interactions*, **29**, 165–169. Available from: https://doi.org/10.1094/mpmi-09-15-0212-fi

Felippes, F.F. & **Weigel, D.** (2009) Triggering the formation of tasiRNAs in *Arabidopsis thaliana*: the role of microRNA miR173. *EMBO Reports*, **10**, 264–270. Available from: https://doi.org/10.1038/embor.2008.247

Fliegert, R., **Gasser, A.** & **Guse, A.H.** (2007) Regulation of calcium signalling by adenine-based second messengers. *Biochemical Society Transactions*, **35**, 109–114. Available from: https://doi.org/10.1042/bst0350109

Gou, X., **Zhong, C.**, **Zhang, P.**, **Mi, L.**, **Li, Y.**, **Lu, W.** ***et al.*** (2022) miR398b and *AtC2GnT* form a negative feedback loop to regulate *Arabidopsis thaliana* resistance against *Phytophthora parasitica*. *The Plant Journal*, **111**, 360–373. Available from: https://doi.org/10.1111/tpj.15792

Horsefield, S., **Burdett, H.**, **Zhang, X.**, **Manik, M.K.**, **Shi, Y.**, **Chen, J.** ***et al.*** (2019) NAD^+ cleavage activity by animal and plant TIR domains in cell death pathways. *Science*, **365**, 793–799. Available from: https://doi.org/10.1126/science.aax1911

Howell, M.D., **Fahlgren, N.**, **Chapman, E.J.**, **Cumbie, J.S.**, **Sullivan, C.M.**, **Givan, S.A.** ***et al.*** (2007) Genome-wide analysis of the RNA-DEPENDENT RNA POLYMERASE6/DICER-LIKE4 pathway in *Arabidopsis* reveals dependency on miRNA-and tasiRNA-directed targeting. *The Plant Cell*, **19**, 926–942. Available from: https://doi.org/10.1105/tpc.107.050062

Huang, G., **Liu, Z.**, **Gu, B.**, **Zhao, H.**, **Jia, J.**, **Fan, G.** ***et al.*** (2019) An RXLR effector secreted by *Phytophthora parasitica* is a virulence factor and triggers cell death in various plants. *Molecular Plant Pathology*, **20**, 356–371. Available from: https://doi.org/10.1111/mpp.12760

Huang, S., **Jia, A.**, **Song, W.**, **Hessler, G.**, **Meng, Y.**, **Sun, Y.** ***et al.*** (2022) Identification and receptor mechanism of TIR-catalyzed small molecules in plant immunity. *Science*, **377**, eabq3297. Available from: https://doi.org/10.1126/science.abq3297

Islam, W., **Noman, A.**, **Qasim, M.** & **Wang, L.** (2018) Plant responses to pathogen attack: small RNAs in focus. *International Journal of Molecular Sciences*, **19**, 515. Available from: https://doi.org/10.3390/ijms19020515

Jacob, P., **Kim, N.H.**, **Wu, F.**, **El-Kasmi, F.**, **Chi, Y.**, **Walton, W.G.** ***et al.*** (2021) Plant "helper" immune receptors are Ca^{2+}-permeable nonselective cation channels. *Science*, **373**, 420–425. Available from: https://doi.org/10.1126/science.abg7917

Jia, A., **Huang, S.**, **Song, W.**, **Wang, J.**, **Meng, Y.**, **Sun, Y.** ***et al.*** (2022) TIR-catalyzed ADP-ribosylation reactions produce signaling molecules for plant immunity. *Science*, **377**, eabq8180. Available from: https://doi.org/10.1126/science.abq8180

Kamoun, S., **Furzer, O.**, **Jones, J.D.G.**, **Judelson, H.S.**, **Ali, G.S.**, **Dalio, R.J.D.** ***et al.*** (2015) The top 10 oomycete pathogens in molecular plant pathology. *Molecular Plant Pathology*, **16**, 413–434. Available from: https://doi.org/10.1111/mpp.12190

Kolodziej, M.C., **Singla, J.**, **Sánchez-Martín, J.**, **Zbinden, H.**, **Šimková, H.**, **Karafiátová, M.** ***et al.*** (2021) A membrane-bound ankyrin repeat protein confers race-specific leaf rust disease resistance in wheat. *Nature Communications*, **12**, 956. Available from: https://doi.org/10.1038/s41467-020-20777-x

Kronmiller, B.A., **Feau, N.**, **Shen, D.**, **Tabima, J.F.**, **Ali, S.S.**, **Armitage, A.D.** ***et al.*** (2023) Comparative genomic analysis of 31 *Phytophthora* genomes reveals genome plasticity and horizontal gene transfer. *Molecular Plant-Microbe Interactions*, **36**, 26–46. Available from: https://doi.org/10.1094/mpmi-06-22-0133-r

Lapin, D., **Johanndrees, O.**, **Wu, Z.**, **Li, X.** & **Parker, J.E.** (2022) Molecular innovations in plant TIR-based immunity signaling. *The Plant Cell*, **34**, 1479–1496. Available from: https://doi.org/10.1093/plcell/koac035

Li, J., **Deng, F.**, **Wang, H.**, **Qiang, X.**, **Meng, Y.** & **Shan, W.** (2022) The Raf-like kinase Raf36 negatively regulates plant resistance against the oomycete pathogen *Phytophthora parasitica* by targeting MKK2. *Molecular Plant Pathology*, **23**, 530–542. Available from: https://doi.org/10.1111/mpp.13176

Li, W., **Zhao, D.**, **Dong, J.**, **Kong, X.**, **Zhang, Q.**, **Li, T.** ***et al.*** (2020) *AtRTP5* negatively regulates plant resistance to *Phytophthora* pathogens by modulating the biosynthesis of endogenous jasmonic acid and salicylic acid. *Molecular Plant Pathology*, **21**, 95–108. Available from: https://doi.org/10.1111/mpp.12883

Li, X., **Kapos, P.** & **Zhang, Y.** (2015) NLRs in plants. *Current Opinion in Immunology*, **32**, 114–121. Available from: https://doi.org/10.1016/j.coi.2015.01.014

Liu, Q., **Zhang, C.**, **Fang, H.**, **Yi, L.** & **Li, M.** (2023) Indispensable biomolecules for plant defense against pathogens: NBS-LRR and "nitrogen pool" alkaloids. *Plant Science*, **334**, 111752. Available from: https://doi.org/10.1016/j.plantsci.2023.111752

López-Márquez, D., **Del-Espino, Á.**, **Ruiz-Albert, J.**, **Bejarano, E.R.**, **Broderson, P.** & **Beuzón, C.R.** (2023) Regulation of plant immunity via small RNA-mediated control of NLR expression. *Journal of Experimental Botany*, **74**, 6052–6068. Available from: https://doi.org/10.1093/jxb/erad268

Lu, W., **Deng, F.**, **Jia, J.**, **Chen, X.**, **Li, J.**, **Wen, Q.** ***et al.*** (2020) The *Arabidopsis thaliana* gene *AtERF019* negatively regulates plant resistance to *Phytophthora parasitica* by suppressing PAMP-triggered immunity. *Molecular Plant Pathology*, **21**, 1179–1193. Available from: https://doi.org/10.1111/mpp.12971

Luan, Y., **Cui, J.**, **Li, J.**, **Jiang, N.**, **Liu, P.** & **Meng, J.** (2018) Effective enhancement of resistance to *Phytophthora infestans* by overexpression of miR172a and b in *Solanum lycopersicum*. *Planta*, **247**, 127–138. Available from: https://doi.org/10.1007/s00425-017-2773-x

Ma, S., **Lapin, D.**, **Liu, L.**, **Sun, Y.**, **Song, W.**, **Zhang, X.** ***et al.*** (2020) Direct pathogen-induced assembly of an NLR immune receptor complex to form a holoenzyme. *Science*, **370**, eabe3069. Available from: https://doi.org/10.1126/science.abe3069

Ma, Z., **Jiang, J.**, **Hu, Z.**, **Lyu, T.**, **Yang, Y.**, **Jiang, J.** ***et al.*** (2017) Overexpression of miR158 causes pollen abortion in *Brassica campestris* ssp. chinensis. *Plant Molecular Biology*, **93**, 313–326. Available from: https://doi.org/10.1007/s11103-016-0563-7

Martin, R., **Qi, T.**, **Zhang, H.**, **Liu, F.**, **King, M.**, **Toth, C.** ***et al.*** (2020) Structure of the activated ROQ1 resistosome directly recognizing the pathogen effector XopQ. *Science*, **370**, eabd9993. Available from: https://doi.org/10.1126/science.abd9993

Maruta, N., **Burdett, H.**, **Lim, B.Y.J.**, **Hu, X.**, **Desa, S.**, **Manik, M.K.** ***et al.*** (2022) Structural basis of NLR activation and innate immune signalling in plants. *Immunogenetics*, **74**, 5–26. Available from: https://doi.org/10.1007/s00251-021-01242-5

Meyers, B.C., **Morgante, M.** & **Michelmore, R.W.** (2002) TIR-X and TIR-NBS proteins: two new families related to disease resistance TIR-NBS-LRR proteins encoded in *Arabidopsis* and other plant genomes. *The Plant Journal*, **32**, 77–92. Available from: https://doi.org/10.1046/j.1365-313x.2002.01404.x

Nandety, R.S., **Caplan, J.L.**, **Cavanaugh, K.**, **Perroud, B.**, **Wroblewski, T.**, **Michelmore, R.W.** ***et al.*** (2013) The role of TIR-NBS and TIR-X proteins in plant basal defense responses. *Plant Physiology*, **162**, 1459–1472. Available from: https://doi.org/10.1104/pp.113.219162

Nasim, Z., **Fahim, M.**, **Gawarecka, K.**, **Susila, H.**, **Jin, S.**, **Youn, G.** ***et al.*** (2020) Role of *AT1G72910*, *AT1G72940*, and *ADR1-LIKE 2* in plant immunity under nonsense-mediated mRNA decay-compromised conditions at low temperatures. *International Journal of Molecular Sciences*, **21**, 7986. Available from: https://doi.org/10.3390/ijms21217986

Nimma, S., **Gu, W.**, **Maruta, N.**, **Li, Y.**, **Pan, M.**, **Saikot, F.K.** ***et al.*** (2021) Structural evolution of TIR-domain signalosomes. *Frontiers in Immunology*, **12**, 784484. Available from: https://doi.org/10.3389/fimmu.2021.784484

Pan, Q., **Cui, B.**, **Deng, F.**, **Quan, J.**, **Loake, G.J.** & **Shan, W.** (2016) *RTP1* encodes a novel endoplasmic reticulum (ER)-localized protein in *Arabidopsis* and negatively regulates resistance against biotrophic pathogens. *New Phytologist*, **209**, 1641–1654. Available from: https://doi.org/10.1111/nph.13707

Qi, D., **Dubiella, U.**, **Kim, S.H.**, **Sloss, D.I.**, **Dowen, R.H.**, **Dixon, J.E.** ***et al.*** (2014) Recognition of the protein kinase AVRPPHB SUSCEPTIBLE1 by the disease RESISTANCE protein RESISTANCE TO PSEUDOMONAS SYRINGAE5 is dependent on s-acylation and an exposed loop in AVRPPHB SUSCEPTIBLE1. *Plant Physiology*, **164**, 340–351. Available from: https://doi.org/10.1104/pp.113.227686

Roth, C., **Lüdke, D.**, **Klenke, M.**, **Quathamer, A.**, **Valerius, O.**, **Braus, G.H.** ***et al.*** (2017) The truncated NLR protein TIR-NBS13 is a MOS6/IMPORTIN-α3 interaction partner required for plant immunity. *The Plant Journal*, **92**, 808–821. Available from: https://doi.org/10.1111/tpj.13717

Saile, S.C., **Jacob, P.**, **Castel, B.**, **Jubic, L.M.**, **Salas-Gonzales, I.**, **Baecker, M.** ***et al.*** (2020) Two unequally redundant "helper" immune receptor

families mediate *Arabidopsis thaliana* intracellular "sensor" immune receptor functions. *PLoS Biology*, **18**, e3000783. Available from: https://doi.org/10.1371/journal.pbio.3000783

Schwab, R., **Ossowski, S.**, **Riester, M.**, **Warthmann, N.** & **Weigel, D.** (2006) Highly specific gene silencing by artificial microRNAs in *Arabidopsis*. *The Plant Cell*, **18**, 1121–1133. Available from: https://doi.org/10.1105/tpc.105.039834

Sharma, S., **Sundaresha, S.** & **Bhardwaj, V.** (2021) Biotechnological approaches in management of oomycetes diseases. *3 Biotech*, **11**, 274. Available from: https://doi.org/10.1007/s13205-021-02810-y

Song, L., **Fang, Y.**, **Chen, L.**, **Wang, J.** & **Chen, X.** (2021) Role of non-coding RNAs in plant immunity. *Plant Communications*, **2**, 100180. Available from: https://doi.org/10.1016/j.xplc.2021.100180

Song, W., **Liu, L.**, **Yu, D.**, **Bernardy, H.**, **Jirschitzka, J.**, **Huang, S.** ***et al.*** (2024) Substrate-induced condensation activates plant TIR domain proteins. *Nature*, **627**, 847–853. Available from: https://doi.org/10.1038/s41586-024-07183-9

Sun, L., **Yang, Y.**, **Pan, H.**, **Zhu, J.**, **Zhu, M.**, **Xu, T.** ***et al.*** (2022) Molecular characterization and target prediction of candidate miRNAs related to abiotic stress responses and/or storage root development in sweet potato. *Genes (Basel)*, **13**, 110. Available from: https://doi.org/10.3390/genes13010110

Sun, T., **Zhang, Y.**, **Li, Y.**, **Zhang, Q.**, **Ding, Y.** & **Zhang, Y.** (2015) ChIP-seq reveals broad roles of SARD1 and CBP60g in regulating plant immunity. *Nature Communications*, **6**, 10159. Available from: https://doi.org/10.1038/ncomms10159

Sun, X., **Lapin, D.**, **Feehan, J.M.**, **Stolze, S.C.**, **Kramer, K.**, **Dongus, J.A.** ***et al.*** (2021) Pathogen effector recognition-dependent association of NRG1 with EDS1 and SAG101 in TNL receptor immunity. *Nature Communications*, **12**, 3335. Available from: https://doi.org/10.1038/s41467-021-23614-x

Thines, M. (2018) Oomycetes. *Current Biology*, **28**, R812–R813. Available from: https://doi.org/10.1016/j.cub.2018.05.062

Tripathi, A.M., **Singh, R.**, **Verma, A.K.**, **Singh, A.**, **Mishra, P.**, **Dwivedi, V.** ***et al.*** (2023) Indian Himalayan natural *Arabidopsis thaliana* accessions with abolished miR158 levels exhibit robust miR173-initiated trans-acting cascade silencing. *The Plant Journal*, **114**, 855–874. Available from: https://doi.org/10.1111/tpj.16175

Wan, L., **Essuman, K.**, **Anderson, R.G.**, **Sasaki, Y.**, **Monteiro, F.**, **Chung, E.-H.** ***et al.*** (2019) TIR domains of plant immune receptors are NAD^+-cleaving enzymes that promote cell death. *Science*, **365**, 799–803. Available from: https://doi.org/10.1126/science.aax1771

Wang, J., **Yang, X.**, **Xu, H.**, **Chi, X.**, **Zhang, M.** & **Hou, X.** (2012) Identification and characterization of microRNAs and their target genes in *Brassica oleracea*. *Gene*, **505**, 300–308. Available from: https://doi.org/10.1016/j.gene.2012.06.002

Wang, W., **Feng, B.**, **Zhou, J.-M.** & **Tang, D.** (2020) Plant immune signaling: advancing on two frontiers. *Journal of Integrative Plant Biology*, **62**, 2–24. Available from: https://doi.org/10.1111/jipb.12898

Wang, W., **Liu, N.**, **Gao, C.**, **Rui, L.**, **Jiang, Q.**, **Chen, S.** ***et al.*** (2021) The truncated TNL receptor TN2-mediated immune responses require ADR1 function. *The Plant Journal*, **108**, 672–689. Available from: https://doi.org/10.1111/tpj.15463

Wang, W., **Liu, N.**, **Gao, C.**, **Rui, L.** & **Tang, D.** (2019) The *Pseudomonas syringae* effector AvrPtoB associates with and ubiquitinates *Arabidopsis* exocyst subunit EXO70B1. *Frontiers in Plant Science*, **10**, 1027. Available from: https://doi.org/10.3389/fpls.2019.01027

Wang, Y., **Liu, W.**, **Shen, H.**, **Zhu, X.**, **Zhai, L.**, **Xu, L.** ***et al.*** (2015) Identification of radish (*Raphanus sativus* L.) miRNAs and their target genes to explore miRNA-mediated regulatory networks in lead (Pb) stress responses by high-throughput sequencing and degradome analysis. *Plant Molecular Biology Reporter*, **33**, 358–376. Available from: https://doi.org/10.1007/s11105-014-0752-y

Wang, Y., **Meng, Y.**, **Zhang, M.**, **Tong, X.**, **Wang, Q.**, **Sun, Y.** ***et al.*** (2011) Infection of *Arabidopsis thaliana* by *Phytophthora parasitica* and identification of variation in host specificity. *Molecular Plant Pathology*, **12**, 187–201. Available from: https://doi.org/10.1111/j.1364-3703.2010.00659.x

Williams, S.J., **Sohn, K.H.**, **Wan, L.**, **Bernoux, M.**, **Sarris, P.F.**, **Segonzac, C.** ***et al.*** (2014) Structural basis for assembly and function of a heterodimeric plant immune receptor. *Science*, **344**, 299–303. Available from: https://doi.org/10.1126/science.1247357

Xia, R., **Meyers, B.C.**, **Liu, Z.**, **Beers, E.P.**, **Ye, S.** & **Liu, Z.** (2013) Micro-RNA superfamilies descended from miR390 and their roles in secondary small interfering RNA biogenesis in eudicots. *The Plant Cell*, **25**, 1555–1572. Available from: https://doi.org/10.1105/tpc.113.110957

Xu, M.Y., **Dong, Y.**, **Zhang, Q.X.**, **Zhang, L.**, **Luo, Y.Z.**, **Sun, J.** ***et al.*** (2012) Identification of miRNAs and their targets from *Brassica napus* by high-throughput sequencing and degradome analysis. *BMC Genomics*, **13**, 421. Available from: https://doi.org/10.1186/1471-2164-13-421

Yang, Y., **Zhao, Y.**, **Zhang, Y.**, **Niu, L.**, **Li, W.**, **Lu, W.** ***et al.*** (2022) A mitochondrial RNA processing protein mediates plant immunity to a broad spectrum of pathogens by modulating the mitochondrial oxidative burst. *The Plant Cell*, **34**, 2343–2363. Available from: https://doi.org/10.1093/plcell/koac082

Yoshikawa, M., **Iki, T.**, **Numa, H.**, **Miyashita, K.**, **Meshi, T.** & **Ishikawa, M.** (2016) A short open reading frame encompassing the microRNA173 target site plays a role in trans-acting small interfering RNA biogenesis. *Plant Physiology*, **171**, 359–368. Available from: https://doi.org/10.1104/pp.16.00148

Zhang, X., **Henriques, R.**, **Lin, S.-S.**, **Niu, Q.-W.** & **Chua, N.-H.** (2006) *Agrobacterium*-mediated transformation of *Arabidopsis thaliana* using the floral dip method. *Nature Protocols*, **1**, 641–646. Available from: https://doi.org/10.1038/nprot.2006.97

Zhang, Y. & **Li, X.** (2019) Salicylic acid: biosynthesis, perception, and contributions to plant immunity. *Current Opinion in Plant Biology*, **50**, 29–36. Available from: https://doi.org/10.1016/j.pbi.2019.02.004

Zhao, T., **Rui, L.**, **Li, J.**, **Nishimura, M.T.**, **Vogel, J.P.**, **Liu, N.** ***et al.*** (2015) A truncated NLR protein, TIR-NBS2, is required for activated defense responses in the *exo70B1* mutant. *PLoS Genetics*, **11**, e1004945. Available from: https://doi.org/10.1371/journal.pgen.1004945

Zhong, C. (2019) *Identification and functional characterization of Arabidopsis small RNAs in response to Phytophthora infection* (PhD thesis). Yangling: The Northwest A&F University.